

Tectonic block motion and glacial isostatic adjustment in southeast Alaska and adjacent Canada constrained by GPS measurements

Julie L. Elliott,¹ Christopher F. Larsen,¹ Jeffrey T. Freymueller,¹ and Roman J. Motyka¹

Received 16 November 2009; revised 9 March 2010; accepted 6 April 2010; published 21 September 2010.

[1] We use data from campaign and continuous GPS sites in southeast Alaska and the neighboring region of Canada to constrain a regional tectonic block model that estimates block angular velocities and derives a self-consistent set of fault slip rates from the block motions. Present-day tectonics in southeast Alaska is strongly influenced by the collision of the Yakutat block. Our model predicts a velocity of 50.3 ± 0.8 mm/a toward $N22.9 \pm 0.6^\circ$ W for that block. Our results suggest that the eastern edge of the Yakutat block is deforming. Along this edge, the Fairweather fault accommodates a large portion of the Pacific-North America relative plate motion through 42.9 ± 0.9 mm/a of dextral slip. Further south along the Queen Charlotte fault, our model predicts an average of 43.9 ± 0.6 mm/a of dextral slip and a southward increasing amount of transpression. Strain from the Yakutat collision is transferred far to the east of the strike-slip system. This strain transfer causes the region north of Glacier Bay to undergo a clockwise rotation. South of Glacier Bay and inboard of the Queen Charlotte fault, a smaller but clearly defined clockwise rotation is observed. The heterogeneous block motion north and south of Glacier Bay may indicate the area is undergoing internal deformation and could explain regional patterns of diffuse seismicity. The Northern Cordillera of Canada displays a small northeasterly motion. Our block model suggests that the entire southeastern Alaska-northwestern Canada margin is mobile.

Citation: Elliott, J. L., C. F. Larsen, J. T. Freymueller, and R. J. Motyka (2010), Tectonic block motion and glacial isostatic adjustment in southeast Alaska and adjacent Canada constrained by GPS measurements, *J. Geophys. Res.*, 115, B09407, doi:10.1029/2009JB007139.

1. Introduction

[2] Southeast Alaska and the adjacent portion of north-west Canada form an important segment of the Pacific-North America plate boundary, marking the beginning of the transition from a transform margin to subduction along the Aleutian megathrust (Figure 1). The tectonics of this region is greatly complicated by the Yakutat block's collision with and accretion to southern Alaska. In the southern part of this area the plate boundary is fairly simple, with the dextral Fairweather – Queen Charlotte fault system accommodating the majority of the relative motion [Mazzotti *et al.*, 2003]. From Chatham Strait northward, however, the distribution of relative motion is unclear. The partitioning of motion between onshore and offshore faults is a major question. Several studies suggested that the effects of the Yakutat collision are far-reaching [e.g., Leonard *et al.*, 2007, 2008; Mazzotti *et al.*, 2008], but the available GPS data did not allow the detailed resolution of deformation inboard of the coast.

[3] In this paper, we present a new, larger GPS data set and use that data to develop a tectonic block model for southeastern Alaska and the neighboring part of Canada. We also present an updated version of the southeast Alaska glacial isostatic adjustment model of Larsen *et al.* [2005] and apply the horizontal model predictions to our data. A block model divides a region with complex, varied deformation patterns into a set of rigid blocks whose motion can then be calculated. Using a block model allows us to create a kinematically consistent model that accounts for both long-term tectonic block motion and the transient effects of interseismic strain accumulation on the block-bounding faults [e.g., Meade and Hager, 1999; McCaffrey, 2002; Meade and Hager, 2005]. This approach avoids inconsistencies that can arise when fault slip rates or block velocities are estimated individually.

[4] The improved GPS data set and the block model technique provide a broader perspective on the problem of how the relative motion between the Pacific plate and North America is distributed in this region. Using poles and rotation rates from the block model, we calculate relative rates of motion between the blocks and evaluate what these mean in terms of seismic hazard and strain transfer into adjoining tectonic regions. Particular attention is paid to the question of how relative motion is partitioned between onshore and offshore faults and what this might imply about fragmentation of both the Yakutat block and the Pacific plate. Examining

¹Geophysical Institute, University of Alaska Fairbanks, Fairbanks, Alaska, USA.

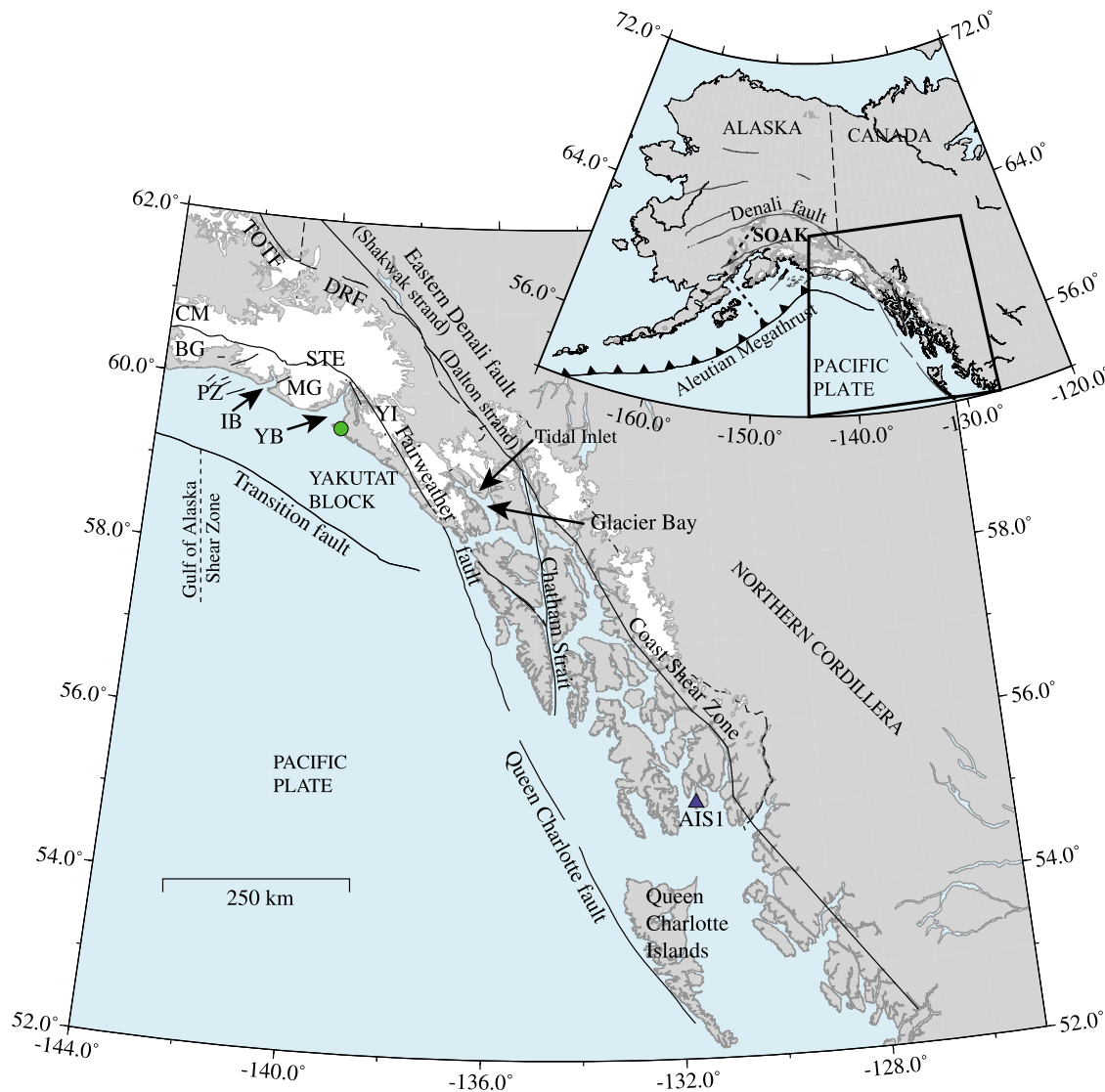


Figure 1. Tectonic setting of southeast Alaska. Green dot marks the city of Yakutat. Abbreviations are CM, Chugach Mountains; BG, Bering Glacier; PZ, Pamplona fault zone; IB, Icy Bay; MG, Malaspina Glacier; STE, St. Elias Mountains; YB, Yakutat Bay; YI, Yakutat ice field; DRF, Duke River fault; TOTF, Totschunda fault; and SOAK, Southern Alaska block. Faults are based on *Plafker et al.* [1994b], *Brew and Ford* [1998], and *Pegler and Das* [1996].

the deformation patterns inboard of the strike-slip system also allows us to assess how much of the present-day eastern Alaska – western Canada margin is mobile.

2. Tectonic Setting

[5] The Yakutat block is a wedge-shaped allochthonous terrane that originated during the mid-Cenozoic as part of what is now the Pacific Northwest [Bruns, 1983] or British Columbia and southeastern Alaska [Plafker et al., 1994a] and traveled north along the Fairweather – Queen Charlotte transform system. It arrived and began colliding with southern Alaska by the late Miocene, roughly 6–10 Ma [Lagoe et al., 1993; Ferris et al., 2003]. The present-day motion of the Yakutat block has been a matter of debate. Some studies have concluded that the Yakutat block moves mainly with

the Pacific plate with little or no relative motion between the two [e.g., Plafker et al., 1994a; Bruns, 1983] while others have suggested that significant Pacific plate – Yakutat block relative motion exists [e.g., Fletcher and Freymueller, 1999; Perez and Jacob, 1980].

[6] The dextral Fairweather–Queen Charlotte fault system is a major tectonic feature of southeast Alaska and accommodates most of the Pacific – North America relative plate motion. The Fairweather fault is usually taken to be the eastern boundary of the Yakutat block [Plafker et al., 1978; Lahr and Plafker, 1980]. The fault extends from the vicinity of Yakutat Bay to Chatham Strait, where it is postulated to connect with the Queen Charlotte fault [Plafker et al., 1994a]. Several $M_w > 7$ earthquakes have occurred along the fault during the past century (Figure 2). In 1958, a $M_w 7.9$ earthquake occurred just north of Cross Sound [Doser and Lomas,

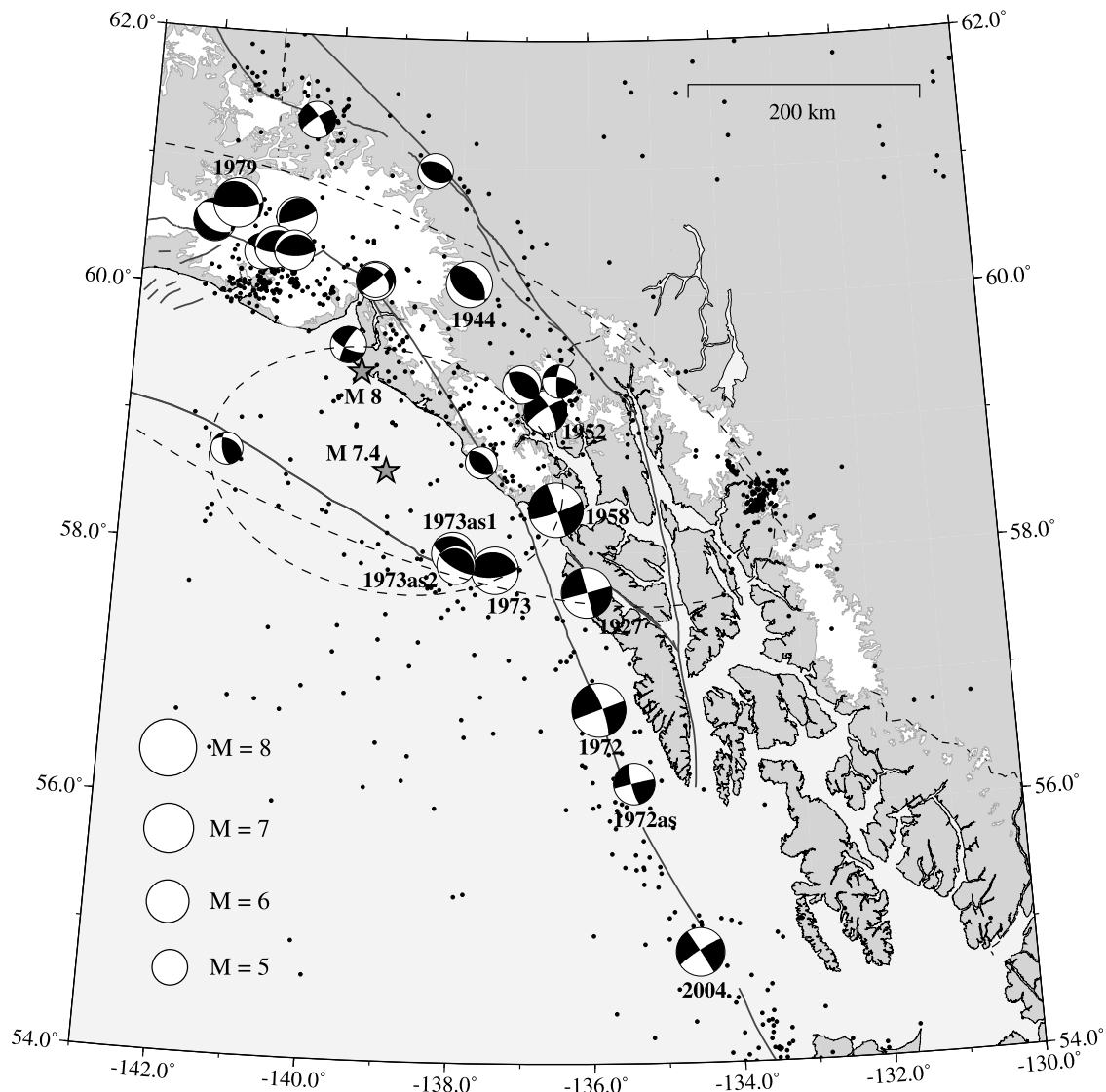


Figure 2. Seismicity in southeastern Alaska and the adjacent region of Canada. Seismic events with $M \geq 3$ are shown by dots and are taken from the AEIC catalog. Available focal mechanisms are shown for $M \geq 4.5$ events. $M \geq 6$ events and their aftershocks are labeled with the year in which they occurred. Focal mechanisms are from *Doser and Lomas* [2000] and the AEIC database (N. Ruppert, personal communication, 2008). Stars indicate the epicenters of the 10 September 1899 events as relocated by *Doser* [2006]. Dashed ellipses indicate uncertainty limits for the relocations. The cluster of earthquakes located east of -134° is not of tectonic origin; they are either glacial or groundwater related events [*Wolf et al.*, 1997].

2000]. The earthquake resulted in well-documented dextral slip of up to 3.5 m and the onshore surface rupture extended over 200 km to at least the northern end of Yakutat Bay [*Plafker et al.*, 1978]. In 1972, the $M_w 7.6$ Sitka earthquake ruptured 180 km offshore the Alexander archipelago [*Doser and Lomas*, 2000; *Schell and Ruff*, 1989]. A $M_w 7$ earthquake in 1927 occurred in the region between the ruptures of the two larger earthquakes [*Doser and Lomas*, 2000]. Geologic and geodetic slip rate estimates for the Fairweather fault range from 41–58 mm/a [*Plafker et al.*, 1978; *Lisowski et al.*, 1987; *Fletcher and Freymueller*, 2003]. A segment of the Queen Charlotte fault located south of our study area generated a

$M_w 8.1$ right-lateral strike-slip earthquake in 1949. In 2004, a $M_w 6.8$ event occurred near the northern end of the fault.

[7] Perhaps the most enigmatic tectonic feature in southeast Alaska, the Transition fault forms the southern boundary of the Yakutat block. Based on undisturbed sediments seen in seismic reflection data, *Bruns* [1983] concluded that the Transition fault has been inactive since the Pliocene and is a fossil fracture zone. In 1973, a series of earthquakes occurred outboard of Cross Sound near the southeastern edge of the Transition fault (Figure 2). The $M_s 6.7$ main shock and the two largest aftershocks had focal mechanisms consistent with thrust/reverse faulting on a fault dipping to the northeast

[Doser and Lomas, 2000]. Perez and Jacob [1980] estimated that the Transition fault accommodates about 10 mm/a of N30°E directed convergence between the Pacific plate and Yakutat block based on seismic slip vectors. The block model of Lahr and Plafker [1980] included 4 mm/a of Pacific plate – Yakutat block relative motion across a dextral/oblique Transition fault. A GPS study by Fletcher and Freymueller [1999] found that ~20 mm/a of Yakutat – Pacific relative convergence must be accommodated on an offshore fault, with the Transition fault suggested as the obvious candidate. Deriving a Yakutat block rotation pole from a small network of GPS velocities and fault azimuth data, Pavlis *et al.* [2004] estimated nearly pure thrust motion along the Transition fault at rates increasing from about 10 mm/a at the southeast end to more than 30 mm/a at the northwestern end. Gulick *et al.* [2007] reported on seismic reflection and bathymetric data that implies the eastern end of the Transition fault has developed into a strike-slip fault. A tectonic model in that study suggested that the entire fault accommodates 10 mm/a or less relative plate motion. Wide-angle seismic data and seismic reflection profiles collected across the Transition fault offshore Yakutat Bay in 2008 indicate that the major, developed structure is nearly vertical and thus likely to be a strike-slip fault if it is active (G. Christeson, personal communication, 2009).

[8] Southeast Alaska and the adjacent region of Canada exhibit several distinct seismicity trends inboard of the Fairweather–Queen Charlotte system. A band of small earthquakes follows the trace of the Duke River fault [Horner, 1983; Mazzotti *et al.*, 2008] (Figure 2), suggesting that it may be involved in the distribution of the relative plate motions. The eastern Denali fault shows low levels of seismicity between the Duke River fault and Chatham strait. No seismic activity is seen along the Chatham Strait fault [Horner, 1983; Mazzotti *et al.*, 2008] (Figure 2).

[9] A trend of seismicity is also found across the Glacier Bay region between the Fairweather and eastern Denali faults. Horner [1983] suggested that the seismicity and high uplift rates observed in Glacier Bay indicated the presence of convergence across the Fairweather fault. Using a model constrained by raised shoreline dating, tide gauge data, and GPS measurements, Larsen *et al.* [2005] concluded that the high uplift rates seen in Glacier Bay are due to glacial isostatic adjustment, not tectonics. Seismicity in this region has consisted of mostly smaller events, with only one possible $M \geq 6$ earthquake recorded east of the Fairweather fault. Doser and Lomas [2000] interpret that event, a M6.0 earthquake in 1952, as a right-lateral strike-slip event that may have occurred on the Border Ranges fault east of the Fairweather fault. Several smaller, $M \geq 4.5$ earthquakes have also occurred in this area in the recent past and the available focal mechanisms show a mixture of strike-slip and thrust events (Figure 2).

[10] Further to the north, a series of very large earthquakes occurred between Icy Bay and Yakutat Bay in September 1899. A $M_s 7.9$ event on September 4 preceded a $M_s 7.4$ foreshock and a $M_s 8.0$ main shock on September 10 [Doser, 2006]. The September 10 main shock generated the largest known onshore coseismic vertical displacement, 14 m of uplift near the head of Yakutat Bay [Tarr and Martin, 1912]. The analysis of Doser [2006] suggests that the September 10 foreshock occurred offshore southeast Alaska

and possibly involved the Transition fault while the main shock occurred near Yakutat Bay and may have ruptured onshore thrust faults (Figure 2). Doser [2006] located the September 4 event within the Pamplona thrust zone to the west of Icy Bay.

3. GPS Data and Analysis

3.1. Data Set

[11] We use GPS data collected at 102 sites in southeast Alaska, Yukon Territory, and British Columbia (Table S1a).¹ Four of the sites are continuously running GPS sites; the other 98 are campaign sites. The continuous GPS sites have operated for 6–10 years. The campaign sites each have between 2 and 11 visits and the time span between first and last visits ranges from 4 to 15 years (Table S2). Much of the campaign data is an extension of the data set presented by Larsen *et al.* [2005]. Many of the velocities reported in that study now have been enhanced by at least one additional occupation. We also use data from several Canadian Base Network sites and augment data we collected at some campaign sites with data collected at those sites by Geomatics Canada and the Pacific Geoscience Centre, Geological Survey of Canada [Leonard *et al.*, 2007; Henton *et al.*, 2006].

3.2. Data Processing and Velocity Estimation

[12] We used the GIPSY/OASIS GOA4 software developed by the Jet Propulsion Laboratory (JPL) [Zumberge *et al.*, 1997] to analyze the GPS data presented here. Data from each day were analyzed separately to create daily loosely constrained frame-free solutions. For data collected prior to 1995, we combined the Alaska data with data from global International GPS Service (IGS) sites and estimated orbits. For data collected from 1995 onwards, we used JPL's fiducial-free orbits. We transformed the daily solutions into the International Terrestrial Reference Frame 2000 (ITRF2000, realization IGSb00). We used ITRF2000 rather than the more recent ITRF2005 because of our need to express our solutions in a North America-fixed frame. We consider the estimate of Sella *et al.* [2007] to be the most reliable determination of the motion of North America as it is based on substantially more data than any other estimate and considers the effects of glacial isostatic adjustment. The estimate of Sella *et al.* [2007] is based on ITRF2000 (IGSb00) and should not be used with ITRF2005 due to differences between the frames. The daily solutions were combined in a linear least squares inversion to estimate velocities at each GPS site.

[13] In our uncertainty estimates, we included uncertainties in the definition of the North America-fixed frame and in the geocenter stability of ITRF in addition to the formal errors in site velocities. The ITRF2000 and ITRF2005 frames differ by a ~ 1.8 mm/a geocenter translation along the spin axis (Z axis). At the latitudes considered in this study, the geocenter difference results in a velocity difference of ~ 1 mm/a in the north component and ~ 1 mm/a in the vertical component. Argus [2007] and Kogan and Steblov [2008] both attempted to estimate a geocenter correction to ITRF. The result of Argus [2007] lies between ITRF2000 and ITRF2005

¹Auxiliary materials are available in the HTML. doi:10.1029/2009JB007139.

while *Kogan and Steblov* [2008]’s result is closer to ITRF2000. Since we do not know if either frame is correct, we augmented the velocity uncertainties by 1.8 mm/a in the Z component, which reduces the weight given to the north and vertical velocity components accordingly. The impact of any small bias in the velocities on the model results in this paper is very small. The use of ITRF2000 in both our velocity estimates and our choice of reference plate pole minimizes the bias. Further details about the processing, velocity estimation, and the augmentation of uncertainties due to possible systematic errors can be found in the work of *Frey Mueller et al.* [2008].

3.3. Coseismic and Postseismic Effects

[14] The data time span for many sites (Table S2) crosses the date of the 2002 Denali fault earthquake and we applied a correction for the coseismic displacements [*Hreinsdóttir et al.*, 2006] to each station as part of the velocity estimation. The magnitude of the correction ranges from 2 mm to 14 mm across our network, with the larger displacements located in Canada east of the Shakwak strand of the Denali fault (Figure 1). Postseismic deformation from the Denali earthquake is very small for most of the area considered in this study. A robust postseismic deformation model for our study area is not available as published models [*Pollitz*, 2005; *Freed et al.*, 2006; *Johnson et al.*, 2009] significantly overpredict the postseismic effect in the far field. We were able to calculate the difference between the pre-earthquake and post-earthquake velocities at a number of sites in the Northern Cordillera, near the Duke River fault, and in the city of Yakutat (Figure 1). These sites, as the sites closest to the 2002 rupture, would be expected to display the largest postseismic effects. Only the two most northerly sites, Y565 and DEST (Table S1a), displayed differences greater than their 2- σ uncertainty estimates. For these two sites, we used only the pre-earthquake data to determine their velocities. The other sites had differences at or below the 1- σ level. The differences between the pre-earthquake velocities and velocities calculated using both pre- and post-earthquake data were even smaller. For this reason, we used all available data to calculate velocities at the remaining 100 sites in our data set.

[15] We did not correct for the postseismic effects of the 1964 M9.2 Prince William Sound earthquake. Our study area is over 250 km east of the end of that rupture. The model of *Suito and Frey Mueller* [2009] predicts that southeast Alaska sites showing the largest effect, Y565 and the site at Yakutat, have postseismic motion of 0.1 mm/a and 0.2 mm/a, respectively.

[16] We also do not correct for the possible postseismic effects of the 1958 earthquake on the Fairweather fault or the 1899 earthquake sequence. While formal postseismic models do not exist for either the 1899 or 1958 earthquakes, we can estimate the degree to which any postseismic effect from those events would have decayed by the present time. If we assume a shear modulus of 70 GPa (based on PREM [*Dziewonski and Anderson*, 1981]) and an asthenosphere viscosity of 3.7×10^{18} Pa s [*Larsen et al.*, 2005], we obtain a Maxwell relaxation time of ~ 2 years for southeast Alaska. Even if these $\sim M8$ events had considerable initial postseismic effects, they would have decayed into negligible amounts by the present-day. Corroborating this, *Fletcher*

and *Frey Mueller* [2003] used both EDM data collected in the 1980s and GPS data collected in the 1990s in the region of the 1958 rupture and found the two data sets to be compatible. If substantial postseismic effects from the 1958 event were present, the decade time lapse between the data sets should have resulted in apparent differences.

3.4. Glacial Isostatic Adjustment Model

[17] Southeast Alaska has experienced considerable ice volume loss since the end of the Little Ice Age (LIA) in the late 1700s [*Motyka*, 2003; *Larsen et al.*, 2004]. The glacial isostatic adjustment (GIA) due to this ice loss results in the fastest ongoing isostatic uplift measured anywhere [*Larsen et al.*, 2005]. Two uplift centers have been identified with peak uplift rates of 30 mm/a in Glacier Bay and 32 mm/a in the Yakutat ice field. We find that the GIA models discussed below indicate horizontal deformation associated with this ice loss reaches maximum values in excess of 7 mm/a and overprints the regional tectonic deformation pattern. Tectonic interpretation of the regional deformation field relies on first accounting for the GIA horizontal signal. Here we follow the approach of *Larsen et al.* [2005], but use an updated data set and an improved model calculation.

[18] To model the Earth’s viscoelastic response to ice load changes in southeast Alaska, we tested a suite of Earth models in which we varied the effective elastic lithospheric thickness and the viscosity profile of the upper mantle while minimizing misfit between the observations and the predicted uplift. The models presented here use a non-rotating, incompressible, self-gravitating, Maxwell viscoelastic spherically symmetric Earth model and are computed using the TABOO program [*Spada et al.*, 2003; *Spada*, 2003; *Spada et al.*, 2004]. Numerically, this model uses axial-symmetric disks to describe surface loads and both the current models and previously presented models [*Larsen et al.*, 2005] use the same surface load geometry and load history.

[19] In our earth model, we explicitly include a thin, low viscosity asthenosphere overlaying the upper mantle. The density and elastic properties of the Earth model follow the seismic model PREM [*Dziewonski and Anderson*, 1981]. We expanded the spherical harmonics used throughout the numerical modeling to degree and order 2048 in order to resolve small ice load changes and their effects. This is a factor of two greater resolution on the numerical earth modeling compared to the previously presented models [*Larsen et al.*, 2005]. The higher resolution accommodates the denser distribution and greater accuracy of the GPS data and is fully consistent with the 20×20 km resolution of the ice model.

[20] The earth model parameters and the ranges over which we varied them are as follows: lithospheric elastic thickness, 30–120 km, asthenosphere thickness and viscosity, 80–150 km and 1×10^{18} – 5×10^{19} Pa s, and upper mantle viscosity, 1×10^{20} – 5×10^{20} Pa s. Misfit with the observations was found to rapidly increase at the upper and lower limits of all of these parameter ranges. Our GIA model assessments were performed through comparisons of model predictions to vertical GPS velocities, raised shoreline records of RSL (relative sea level), and the tide gauge rates of RSL as described by *Larsen et al.* [2005]. We did not attempt to analyze the horizontal motions resultant from our rebound

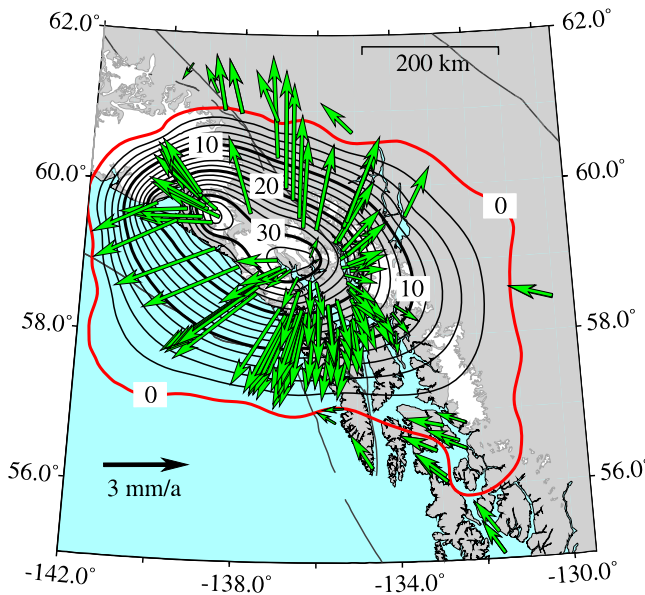


Figure 3. Glacial isostatic adjustment model predictions for southeast Alaska. Vectors show the horizontal motion while the contours show the vertical motion. Contour label units are mm/a (Figure S1 shows a larger version).

models here as has been done in Fennoscandia [Milne *et al.*, 2001], because the dominant horizontal signal observed in southern Alaska is of tectonic origin.

[21] These earth models were subjected to two ice load models simultaneously – one that approximates southern Alaskan and adjoining Canadian glacial history (“Regional”) and another that describes the asynchronous behavior of the Glacier Bay ice field (“Glacier Bay”). Both of these load histories were held fixed in magnitude and timing for all of the rebound model results presented here. Only the last ~2 ka of load histories were considered in our Regional and Glacier Bay load models. Earlier load changes have relatively minimal effects on present-day velocities [Larsen *et al.*, 2005]. Load histories for both the Regional and Glacier Bay ice models are shown in Figure 5 of Larsen *et al.* [2005] and account for both loading and unloading phases of the past 2000 years. The present response is dominated by the unloading phase over approximately the past 100–200 years.

[22] The regional ice load model used here is unchanged from previous studies [Larsen *et al.*, 2005]. It estimates the change in ice volume through the advance and retreat of the LIA [Porter, 1989; Wiles *et al.*, 1999]. The measured rates of volume change [Arendt *et al.*, 2002] were extrapolated to estimate the LIA peak volume in 1900. Earlier volume changes are based on the relative strength of the advance and retreat cycles [Wiles *et al.*, 1999]. We used Neoglacial terminal moraine positions to estimate differential ice volume of these earlier advance and retreat cycles [Larsen *et al.*, 2004], a method that can be problematic in polar systems but is realistic in rapidly adjusting temperate ice systems [Harrison *et al.*, 2003]. The spatial distribution of ice thickness change throughout the load history was allotted according to elevation [Arendt *et al.*, 2002]. The distribution of these thickness changes was gridded at a 20-km × 20-km resolution and assigned a history. This regional ice

load model is based on dendrochronologic and geomorphologic histories of the LIA in southern Alaska [Porter, 1989; Wiles *et al.*, 1999].

[23] We accounted for the large-scale retreat of the Glacier Bay ice field in a separate load model, also unchanged from Larsen *et al.* [2005]. We modeled an ice volume loss of 3030 km³ from the collapse of the ice field, which occurred rapidly (< 250 years beginning ca. 1780 AD) through the process of a tidewater calving retreat. This localized ice wastage represents the largest post-LIA deglaciation known to us. Greater than the volume lost from all Alaskan and neighboring Canadian glaciers between 1955 and 2002 [Arendt *et al.*, 2002], it covered a much smaller area with ice thickness changes of up to 1.5 km [Clague and Evans, 1993]. The volume of ice lost in Glacier Bay along since the end of the LIA is equivalent to a global rise in sea level (SLE) of 8 mm.

[24] The best fit earth model parameters found here are slightly different from those of Larsen *et al.* [2005]: a 50 km (versus 60 km in the previous model) thick lithosphere overlying a 110 km thick asthenosphere of viscosity 3.7×10^{18} Pa s (versus $2.5\text{--}4.0 \times 10^{18}$ Pa s) over an upper mantle with a viscosity of 4×10^{20} Pa s. The best fit model now results in a reduced χ^2 value of 1.29 while the previous model had a reduced χ^2 value of 1.52. These minor differences result from a combination of the expanded degree and order of the spherical harmonics and the increased spatial density and accuracy of the GPS data set used, but do not represent a significant change from earlier results. Specifically, the best fit earth model parameters of Larsen *et al.* [2005] lie within the 95% confidence region of the present estimate. Figure 3 shows the full 3-D deformation field of the modeled GIA motion at selected sites in southeast Alaska, and Table S1b lists the model predictions for each site. Figures S2a and S2b show a comparison between the modeled horizontal GIA motion and our horizontal GPS velocities.

[25] These GIA predictions are subject to the assumptions inherent in the earth models we have invoked as well as to the degree to which the data can constrain the models. We have assumed an incompressible earth model. Árnadóttir *et al.* [2009] showed that an incompressible earth model can underestimate the horizontal velocities associated with GIA by factor of 1.5 when compared to compressible earth models while vertical velocities appear to be largely insensitive to the choice. Because of this contrast in sensitivity, our results could underestimate the GIA horizontal effects while still providing a good fit to the observed vertical velocities.

[26] In order to test the widest range of reasonable predictions of horizontal GIA effects in the tectonic models that follow, we considered two additional models beyond the best fit model. These two models (elastic lithospheric thickness with asthenosphere viscosity: 50 km with 7×10^{18} Pa s, 85 km with 1.5×10^{18} Pa s) lie on opposite edges of the 95% confidence range and represent the greatest allowable variation in model parameters (see Figure 6 of Larsen *et al.* [2005], for description of the misfit distribution). The resulting predictions of the horizontal GIA effects at the sites in our GPS network vary by a factor of two or more in magnitude at some sites and also display considerable variations in azimuth compared to the best fit model (Figure S3). Although we do not explicitly test the effects of our assumption of

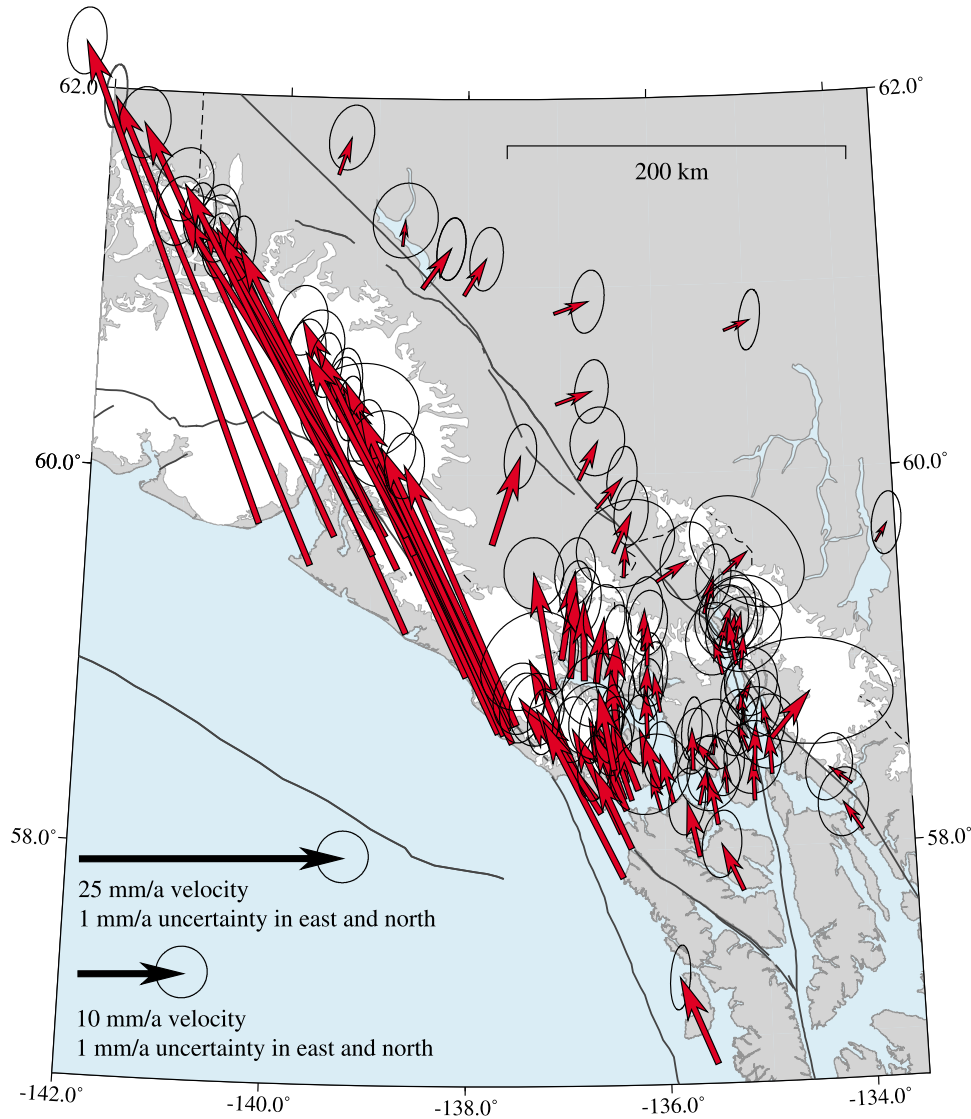


Figure 4. GPS velocities with GIA model predictions applied for southeast Alaska and the adjacent portion of the Canadian Cordillera. Figure S4 shows all of the GPS velocities used in our model.

incompressibility in the earth models, the range of horizontal GIA effects produced by our three test models reasonably accommodates the range of predictions that could be associated with various assumptions of compressibility/incompressibility. In the development of our tectonic block model, we favor the best fit GIA model but also use the two end-member models to gauge their effects on our conclusions.

3.5. Velocity Field

[27] Figure 4 shows the GPS velocities with the predicted horizontal GIA motion removed. Velocities near the Fairweather fault show nearly uniformly northwest-directed motion while velocities closer to the coast display slightly more northerly motion. The largest magnitude velocities, ~ 50 mm/a, border Yakutat Bay, with little difference seen between the magnitudes at sites on the north and south sides of the mouth of the bay. Inboard of the coast, sites between the Fairweather – Queen Charlotte system and Denali fault – Coast Shear zone have comparatively slower velocities and

this portion of the velocity field displays a distinct clockwise rotation. East of the eastern Denali fault, velocities have a nearly uniform northeasterly trend and decrease in magnitude from north to south. East of 130°W longitude, velocities at sites in the Canadian Base Network have very small magnitudes.

4. Block Model

4.1. Modeling Approach

[28] To develop our block model for southeast Alaska and northwest Canada, we adapted the method of *Meade and Hager* [2005]. We present a summary of the method below; further details can be found in their study.

[29] Assuming linear elasticity, we can express the interseismic velocity \vec{v}_I observed at a GPS site as a combination of block motion and elastic effects:

$$\vec{v}_I = \vec{v}_B(\vec{x}_{site}) - \vec{v}_{SD}(\vec{x}_{site}, \vec{x}_{geom}) \quad (1)$$

The GPS site coordinates correspond to \vec{x}_{site} , the fault geometry to \vec{x}_{geom} , and the block velocity to \vec{v}_B . The term \vec{v}_{SD} represents the slip deficit accumulating on a locked fault.

[30] When dealing with block velocities, it is convenient to work in terms of rotations in an earth-centered Cartesian (XYZ) coordinate system. The angular velocities of the blocks are then represented by $\Omega = [\Omega_X, \Omega_Y, \Omega_Z]$. Rewriting the equation for block velocity in terms of Ω yields

$$\vec{v}_B(\vec{x}_{site}) = \vec{\Omega} \times \vec{x}_{site} = \mathbf{R}_B(\vec{x}_{site})\vec{\Omega} \quad (2)$$

where $\mathbf{R}_B(\vec{x}_{site})$ is a linear cross product operator that is a function of the site coordinates.

[31] The slip deficit term can be written as

$$\vec{v}_{SD} = \mathbf{G}(\vec{x}_{site}, \vec{x}_{geom})\vec{s} \quad (3)$$

where \mathbf{G} is the matrix of Green's functions that relate slip, \vec{s} , on each fault plane to the displacement at each GPS site assuming an elastic half-space and a Poisson's ratio of 0.25 [Okada, 1985].

[32] The slip vector is written as

$$\vec{s} = \mathbf{R}_{FP}(\vec{x}_{geom})\mathbf{R}_{X \rightarrow E}(\vec{x}_{geom})\mathbf{R}_{vdiff}(\vec{x}_{geom})\vec{\Omega} \quad (4)$$

$\mathbf{R}_{vdiff}(\vec{x}_{geom})$ takes the angular velocities for two neighboring blocks and calculates their relative velocity at the midpoint of each plane of the fault that divides them. $\mathbf{R}_{X \rightarrow E}(\vec{x}_{geom})$ transforms the relative velocities from the XYZ coordinate system to the ENU system. Finally, $\mathbf{R}_{FP}(\vec{x}_{geom})$ projects the relative velocities into fault parallel and fault perpendicular components. Each fault plane is only allowed two components of slip, either strike-slip and fault normal (contraction or extension) if the fault is vertical or strike-slip and dip-slip if not.

[33] The fault slip rates directly depend on the block angular velocities and the block geometries. Since the slip rates cannot vary independently of each other, the block model ensures that the estimated slip rates are internally consistent (see Figure 2 of Meade *et al.* [2002]).

[34] By substituting (4) into (3) and combining the successive transformations into a single matrix \mathbf{R}_{SD} , (1) can be rewritten as

$$\vec{v}_I = (\mathbf{R}_B - \mathbf{R}_{SD})\vec{\Omega} \quad (5)$$

To include a priori block angular velocities and slip rates in the model, a system of equations can be written as follows:

$$\begin{bmatrix} \vec{v}_I \\ \vec{s}_{apr} \\ \vec{\Omega}_{apr} \end{bmatrix} = \begin{bmatrix} \mathbf{R}_B - \mathbf{R}_{SD} \\ \mathbf{R}_{FP}\mathbf{R}_{X \rightarrow E}\mathbf{R}_{vdiff} \\ \mathbf{I} \end{bmatrix} \vec{\Omega} \quad (6)$$

where \mathbf{I} is the identity matrix.

[35] Equation (6) can be written as

$$\vec{d} = \mathbf{R}\vec{\Omega} \quad (7)$$

where \vec{d} contains the east and north components of the GPS velocities, the a priori slip estimates, and the a priori block angular velocities. This equation allows us to solve for the

block angular velocities $\vec{\Omega}$ through a weighted linear least squares inversion.

$$\vec{\Omega}_{est} = (\mathbf{R}^T \mathbf{W} \mathbf{R})^{-1} \mathbf{R}^T \mathbf{W} \vec{d}$$

where $\mathbf{W}^T \mathbf{W} = \Sigma^{-1}$ and Σ is the data covariance matrix. Besides containing the variance of the observed east and north GPS velocities and the correlations between the east and north components of the GPS data, Σ contains uncertainty estimates for a priori slip rates and block angular velocities. In our implementation, predictions from an a priori model calculated using our a priori block angular velocities (see Section 4.3 below) are subtracted from the data. The estimated angular velocities obtained from the inversion are corrections to that a priori model. Slip rate and linear block velocity uncertainty estimates are calculated by propagating the estimated uncertainty for Ω_{est} through (4) and (2), respectively.

4.2. Block and Fault Geometries

[36] Our block model for southeast Alaska and the neighboring region of Canada includes ten blocks and plates and eleven bounding faults or fault zones (Figure 5). Block boundaries are either recognized faults (through geologic studies or documented seismic activity) or previously postulated faults or fault zones. Locations generally follow mapped traces on geologic maps, seismicity trends, or topography. Due to the region's ruggedness and ice cover, the map traces often represent inferred faults or uncertain locations.

[37] Most of our model faults are well known and based on the map of Plafker *et al.* [1994b], but several of our faults and block designations came from other sources and merit further discussion. Richter and Matson [1971] and Lahr and Plafker [1980] postulated that a connection between the southern end of the Totschunda fault and the Fairweather fault existed. There are a number of NNW-ESE oriented linear valleys in the region that could indicate the presence of a fault. Exposed geological features along the East Nunatak and Art Lewis glaciers east of the Fairweather fault in the Yakutat ice field are compatible with right-lateral slip (G. Plafker, personal communication, 2006). Using geologic slip rates as inputs into a finite element model for southern Alaska, Kalbas *et al.* [2008] concluded that the presence of a connection between the Totschunda and Fairweather faults provided the best explanation of the data. Our modeled Totschunda-Fairweather connector fault branches off the Fairweather fault near the Art Lewis glacier and follows linear, ice-filled valleys northwestward before making a simple connection to the Totschunda fault (Figure 5).

[38] The Chatham Strait fault (Figure 1) would seem like a plausible location for a block boundary as it appears to connect to the Eastern Denali fault [e.g., Lahr and Plafker, 1980], but there is little to no seismicity along that fault (Figure 2). The GPS velocity field (Figure 4) shows no indication of an active fault along the Strait; the velocities instead imply that GPS sites on either side of the Strait belong on the same crustal block. We propose the Coast Shear zone as an alternative block boundary (Figures 1 and 5), following Lanphere [1978], who suggested that the Eastern Denali fault might continue onto the Coast Shear zone instead of the Chatham Strait fault. The Coast Shear zone serves as the general boundary between the western metamorphic belt and the

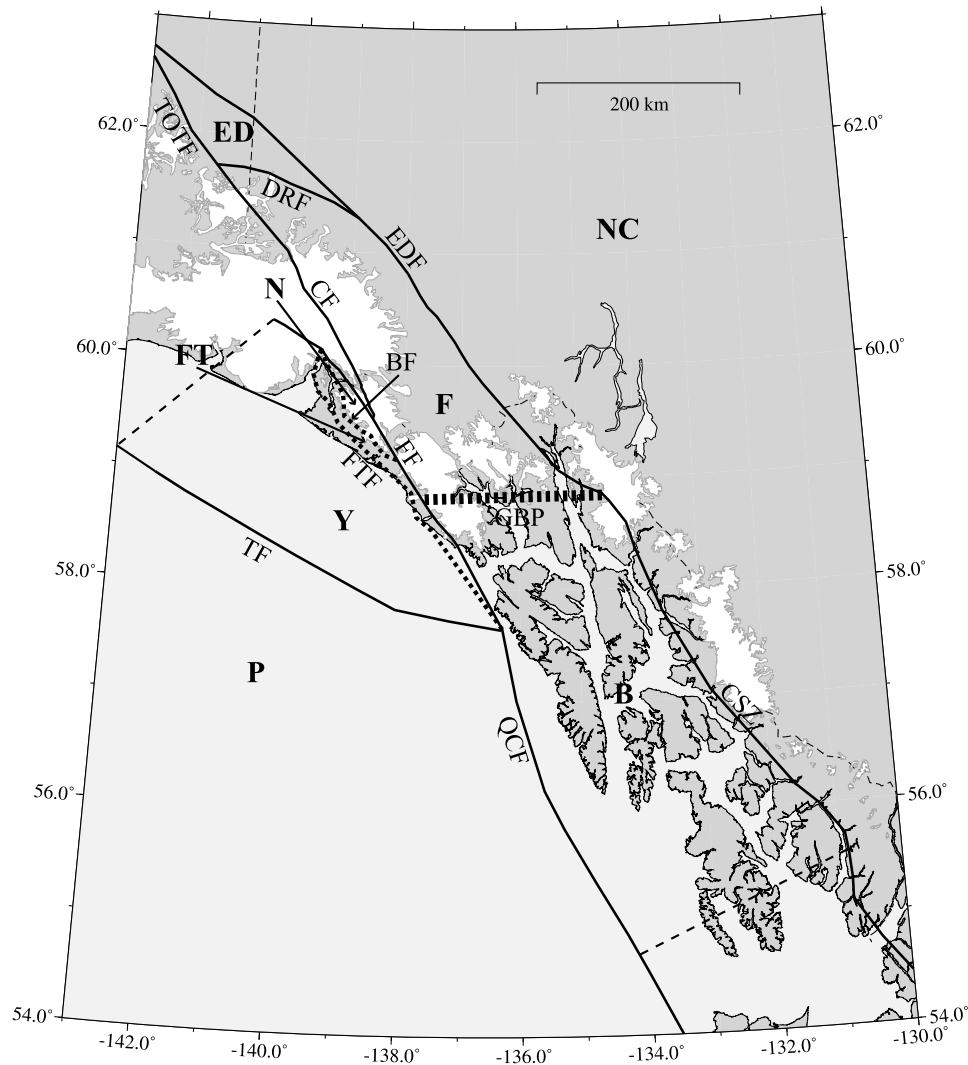


Figure 5. Blocks and bounding faults used in our southeast Alaska inversion model. Bold type indicates a block and regular type indicates a bounding fault. Abbreviations are P, Pacific Plate; Y, Yakutat block; FT, Foothills block; N, Nunatak block; F, Fairweather block; B, Baranof block; ED, Eastern Denali block; NC, Northern Cordillera block; TF, Transition fault; FTF, Foothills fault; BF, Boundary fault; FF, Fairweather fault; QCF, Queen Charlotte fault; CSZ, Coastal Shear zone; GBP, Glacier Bay Partition; EDF, Eastern Denali fault; DRF, Duke River fault; CF, Totschunda–Totschunda Connector fault; and TOTF, Totschunda–Totschunda Connector fault.

Coast Mountains batholith to the east [Brew and Ford, 1998; McClelland *et al.*, 2000, 1992; Klepeis *et al.*, 1998]. Along much of its length, the Coast Shear zone coincides with a tonalite sill belt [Brew and Ford, 1981; Brew, 1994; Brew and Ford, 1998]. Both contraction and dextral transpression appear to have occurred along the Coast Shear zone during early Tertiary time and it may have played a role in strain partitioning during oblique subduction of the Kula plate beneath North America [Rusmore *et al.*, 2001; Klepeis *et al.*, 1998]. McClelland *et al.* [2000] suggested that the Coast Shear zone originated as a strike-slip structure and may have played a role in the evolution of the Denali fault system.

[39] We have subdivided two previously recognized blocks (Yakutat and Fairweather) in order to provide the best fit between the GPS data and our block model. First, we modified the Fairweather block of Fletcher [2002]. The

Duke River fault replaces the northern Eastern Denali fault (Shakwak strand) and the Totschunda and Totschunda–Fairweather connector faults as the northern boundary. A northwest-southeast trending band of seismicity roughly follows the trace of the Duke River fault [Leonard *et al.*, 2007; Horner, 1983] (Figure 2). In contrast, the Shakwak strand shows only sparse present-day seismicity. Paleoseismological evidence obtained from resuspended lake sediments suggests that the Duke River fault and southern Eastern Denali fault (Dalton strand) have been seismically active during the past 300–500 years [Doig, 1998]. This change minimized the misfit between our model and several of the GPS sites in the vicinity of the Duke River fault.

[40] Second, we added two small blocks, the Nunatak block and the Foothills block, along the eastern edge of the Yakutat block. Our initial motivation for including onshore

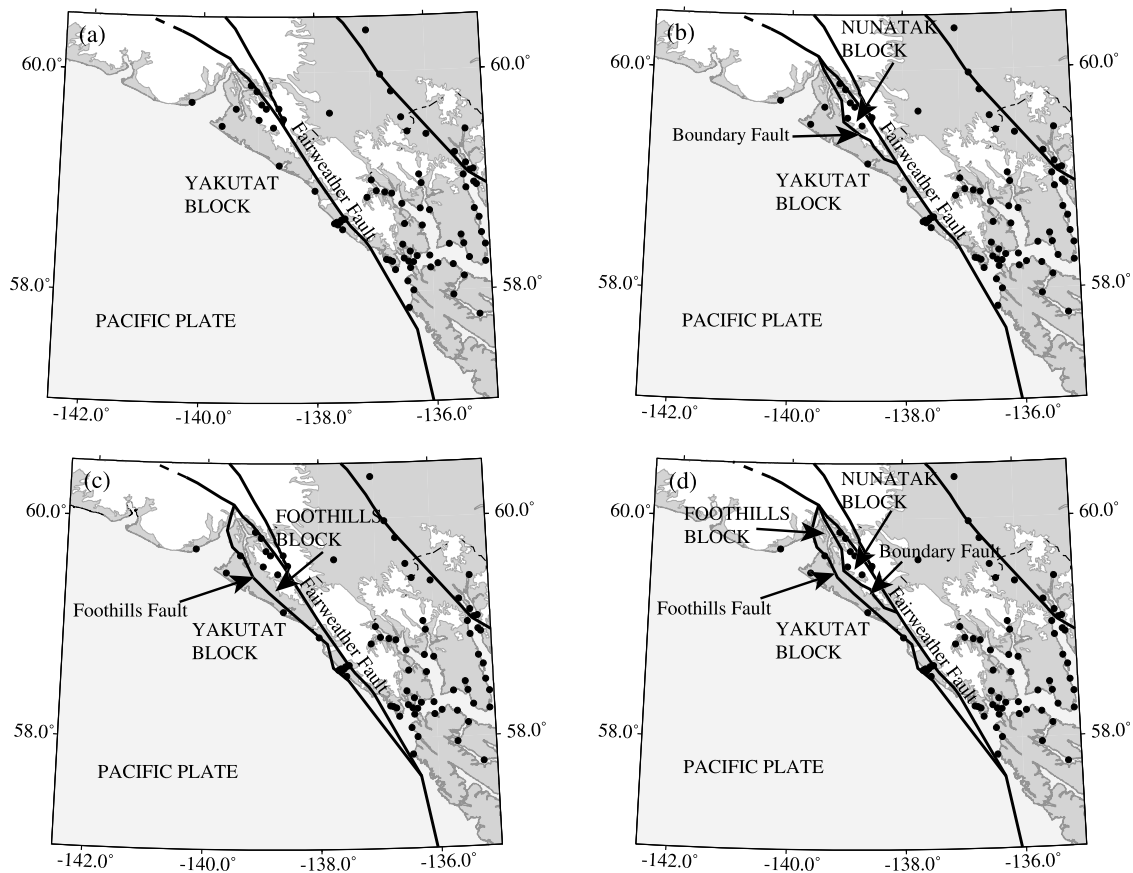


Figure 6. Alternate model geometries without an offshore fault. Black dots show locations of GPS sites. (a) Model without any faults west of the Fairweather fault. (b) Model including the Boundary fault and resulting Nunatak block. (c) Model including the Foothills fault and the resulting Foothills block. (d) Model including the Boundary fault and the Nunatak block as well as the Foothills fault and the Foothills block.

faults along the edge of the Yakutat block was to reduce the unreasonably high rate of convergence (~ 20 mm/a) across the Transition fault predicted by an early version of our block model. As mentioned earlier, recent offshore seismic data suggests that the Transition fault does not have significant thrust fault characteristics. In order to evaluate the compatibility of onshore faults with the GPS data and determine if both offshore and onshore faults were required by the data, we tested a number of alternate fault geometries. For each trial geometry, we performed the inversion, calculated misfit, and ran F-ratio tests to determine the statistical significance of the results. The offshore fault involved was the Transition fault while the onshore faults were the Boundary fault and the Foothills fault. The Boundary fault is a well-known mapped fault while the Foothills fault used here is a modified version of the Yakutat fault of *Plafker and Thatcher* [2008]. We tried four combinations of onshore faults (Figure 6 and Table 1) without an offshore fault as well as several combinations of onshore and offshore faults. Our results show that if no offshore fault is present, including both onshore faults provides the best fit to the data. This model, however, fits more poorly than one with the Transition fault and without either onshore fault. The best fit model has the Transition fault plus both onshore faults, the presence of

which greatly reduced the misfit at sites along the northern Fairweather fault. The addition of each fault to our block model met or exceeded the F test criteria for significance at the 95% level (Table 1). The implications of these faults and blocks are discussed further below.

[41] Finally, our model includes a boundary across Glacier Bay. In the northern Glacier Bay region, structures undergo an abrupt change from north-south strikes to east-west trends [Brew *et al.*, 1978; MacKevett *et al.*, 1971]. This change is particularly obvious at Tidal Inlet, a nearly perfectly east-west trending fjord. MacKevett *et al.* [1971] reported an east-west fault zone here. Brew *et al.* [1978] also noted the presence of a zone of east-west trending faults in the northern section of Glacier Bay and remarked on the unusual orientation. The change in structural strike occurs along the southern edge of observed band of seismicity discussed earlier and separates a more seismically active region in the north from a seismically quiet region to the south. In addition, GPS velocities in the north are generally faster than those in the southern region (Figure 4). We included a boundary, designated the Glacier Bay Partition (GBP), running between the Fairweather and Denali faults through Tidal Inlet, dividing the Fairweather block to the north from the Baranof block to the south. Compared to the best fit model dis-

Table 1. *F* Test Results for Alternative Model Fault Geometries

Model Geometry	χ^2_r	WRSS	P ^a	DoF ^b	F ^c	F Calculated Relative to
1. No Transition fault, no Foothills or Boundary faults	3.6	652.11	18	188	N/A	N/A
2. No Transition fault, no Foothills fault, with Boundary fault	3.26	563.58	21	185	9.58	Model 1
3. No Transition fault, with Foothills fault, no Boundary fault	2.01	361.41	21	185	49.07	Model 1
4. No Transition fault, with Foothills and Boundary faults	1.8	321.24	24	182	7.5	Model 3
5. With Transition fault, no Foothills or Boundary faults	1.54	281.2	21	185	80.46	Model 1
6. With Transition fault, no Foothills fault, with Boundary fault	1.48	267.58	24	182	3.05	Model 5
7. With Transition fault, with Foothills fault, no Boundary fault	1.16	216.75	24	182	17.84	Model 5
8. With Transition fault, Foothills, and Boundary faults	1.09	201.3	27	179	4.52	Model 7
9. With Transition, Foothills, Boundary and GB faults	1.01	184.6	30	176	5.27	Model 8

^aNumber of model parameters.^bDegrees of freedom.^cF value of 2.13 indicates a 90% significance level, F value of 2.66 indicates a 95% significance level, F value of 3.9 indicates a 99% significance level.

cussed in the previous paragraph, the GBP model reduced the overall misfit by $\sim 10\%$ and exceeded the *F* test criteria for significance at the 99% level (Table 1). The GBP is discussed further below.

[42] For our modeling purposes, we assumed that the region north of the central segment of the Denali fault is part of the North American plate. We adopted the Southern Alaska block (SOAK) of *Fletcher* [2002] and assume that block occupies the area south of the Denali-Totschunda system and north of the Chugach and St. Elias Ranges (Figure 1). We defined the region immediately east of the Eastern Denali fault and Coast Shear zone to be the Northern Cordillera block, following *Mazzotti and Hyndman* [2002].

[43] Fault locking depths, dips, and widths in the downdip directions are all fixed; they are not estimated as part of the inversion. We used an iterative process to adjust fault segment endpoints, fault locking depths, and fault width and dip to find the fault geometry that provided the best fit to the GPS data. For each fault, we began with published estimates of the fault geometry, most of which were derived from seismic or geodetic data. If no published estimate or other information was available, we began with a vertical fault with a locking depth of 10 km. If a fault segment had no nearby GPS data to constrain the iterative process, we assigned the fault parameters compatible with neighboring faults. There were two exceptions to this process. The first was the Transition fault. While the northern and central regions were designated as vertical to agree with the offshore seismic reflection data, the southern segment was defined as a steeply dipping thrust fault to agree with the 1973 Cross Sound Earthquakes. The second exception concerns the Boundary and Foothills faults. *Plafker and Thatcher* [2008] used vertical shoreline displacement measurements to constrain a coseismic model for the 1899 earthquakes. In that model, the Boundary fault dips 10° to the NE while the Yakutat fault dips 30° to the NE. Our model Boundary fault dips 85° to the NE and our Foothills fault is vertical. Our model geometries were chosen to minimize both the misfit to the GPS data and the amount of contraction across the Transition fault. These geometries are discussed further below. Table 2 lists fault geometry parameters for the faults used in this model.

4.3. A Priori Block Motion Estimates

[44] Our modeling approach allows the inclusion of a priori block motion estimates. We chose to use a priori block angular velocities for three of the blocks in our model: Pacific, North America, and SOAK. Our data set does not

include any GPS sites on these three blocks, so their inclusion is only important for the calculation of deformation along their boundaries. North America is our reference block – all of our GPS velocities and block angular velocities (estimated and a priori) are relative to it. We used the definition of North America presented by *Sella et al.* [2007]. The GPS data used by *Sella et al.* [2007] to develop this model were aligned with ITRF2000 (IGSb00 realization), so this estimate of North American plate motion will not have reference frame compatibility problems with our GPS velocities. As our a priori Pacific plate motion estimate, we used the GPS-derived angular velocity estimate of *Plattner et al.* [2007], who also used the IGSb00 realization of ITRF2000. We used the pole and rotation rate determined by *Fletcher* [2002] for the motion of SOAK relative to North America. In that model, SOAK rotates counterclockwise about a pole in Prince William Sound. The small circle geometry of the central Denali fault constrains the location of the pole.

[45] Along with the angular velocities, we included uncertainties for the motion of the Pacific plate, North America, and SOAK as a priori information. To ensure numerical stability during the inversion and limit the maxi-

Table 2. Fault Geometry Parameters for Block Model^a

Fault Segment	Fault Width (km)	Locking Depth (km)	Dip (deg)
Totschunda	10	10	90
Duke River	10	10	90
Eastern Denali (Shakwak)	10	10	90
Eastern Denali (Dalton)	10	10	90
Malaspina Fairweather (60.3° – 60°)	5	5	90
Upper Fairweather (60° – 60.5°)	8	7.6	79, to NE
Central Fairweather (59.5° – 57.65°)	10	10	90
Queen Charlotte	10	10	90
Transition (northern and central)	8	8	90
Transition (Cross Sound area)	28.5	26.8	70, to NE
Coast Shear zone	10	10	90
Boundary (60.1° – 59.9°)	8	8	90
Boundary (59.9° – 59.7°)	8	7.96	85, to NE
Boundary (59.7° – 59.5°)	8	8	90
Boundary (59.5° – 59°)	0	0	90
Foothills (60.1° – 58.86°)	8	8	90
Foothills (58.86° – 58.5°)	12	12	90
Foothills (58.5° – 57.65°)	4	4.98	85, to NE
Glacier Bay	8	8	90

^aParameter values are averages for the fault segment. Fault width is measured in the downdip direction.

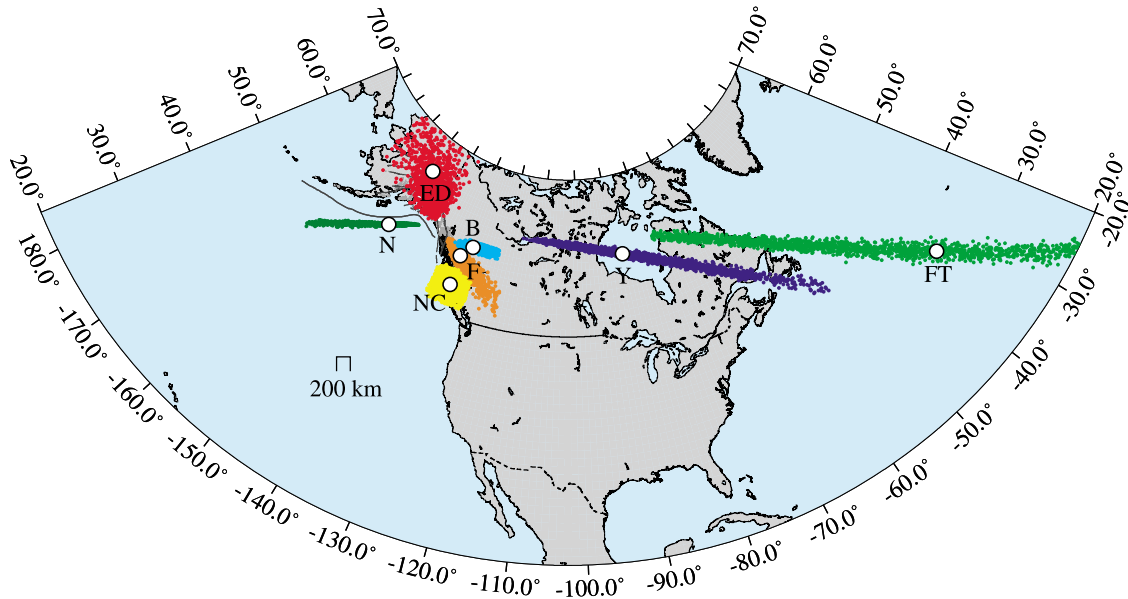


Figure 7. Euler poles and uncertainty clouds for our preferred block model. Uncertainty clouds represent the 95% confidence regions for the pole locations. Abbreviations are ED, Eastern Denali block; N, Nunatak block; F, Fairweather block; B, Baranof block; NC, Northern Cordillera block; Y, Yakutat block; FT, Foothills block. Table 3 lists the locations, rotation rates, angular velocities, and angular velocity covariances for the poles. All poles are relative to the North America definition of *Sella et al.* [2007].

imum rate of vertical axis rotation for small blocks, we also applied loose a priori uncertainties to the estimated angular velocities in our block model. These uncertainties were large, with σ equal to 0.1 radians/Ma.

4.4. A Priori Slip Rate Estimates

[46] With three exceptions, we did not constrain the sense of slip on any of the faults; the slip is solely controlled by the inversion. The first exception is the Eastern Denali fault between the Totschunda and Duke River faults (Shakwak strand), to which we assigned dextral slip of 5 ± 5 mm/a based on recent geologic studies [Seitz et al., 2008]. There are no GPS sites along this part of the fault, so the geologic slip rate estimate is the only data for this segment. For a similar reason, we constrained the Totschunda fault to have 6 ± 6 mm/a of dextral slip following the geologic estimate of Seitz et al. [2008]. Finally, we constrained the Dalton strand of the Eastern Denali fault to have 0 ± 3 mm/a of fault normal motion. We did not constrain the fault parallel motion on this fault. The initial unconstrained iteration of the block model predicted > 5 mm/a of contraction across

this portion of the fault. Previous geodetic and geologic studies [e.g., Fletcher and Freymueller, 2003; Plafker et al., 1994a] have concluded that the fault is primarily a dextral fault, so we considered this rate to be unreasonably high.

5. Results and Interpretation

5.1. Pole and Rotation Rate Estimates

[47] We inverted 246 data (east and north components of GPS velocities at 102 sites, X, Y, and Z components of a priori angular velocities for 10 blocks, and 12 slip constraints) to estimate 21 model parameters (X, Y, and Z components of angular velocity for 7 blocks). We then transformed the estimated angular velocities from the XYZ coordinate system to the geographic coordinate system (longitude, latitude, and rotation rate) in order to present the block rotations in the more familiar Euler pole form. Table 3 and Figure 7 display the Euler poles, rotation rates, angular velocities, block velocity vectors, and associated uncertainties for our preferred block model. Angular velocities for small blocks or blocks without widespread site distributions have a large

Table 3. Poles, Rotation Rates, and Angular Velocities

Block	Latitude (°N)	Longitude (°E)	Rate (deg/Ma)	Omega (X, Y, Z) (10^{-3} rad/Ma)	Omega Covariance (xx, xy, xz, yy, yz, zz) (10^{-6} rad/Ma ²)
Yakutat	59.47	-87.82	-1.04 ± 0.32	-0.35, 9.25, -15.69	5.70, 5.05, -12.73, 4.49, -11.30, 28.47
Fairweather	57.11	-129.89	-0.44 ± 0.18	2.70, 3.23, -6.52	1.44, 1.34, -3.32, 1.26, -3.10, 7.63
Baranof	58.8	-127.67	-0.32 ± 0.09	1.77, 2.29, -4.79	0.35, 0.35, -0.79, 0.34, -0.77, 1.75
N. Cordillera	52.99	-129.58	-0.14 ± 0.03	0.95, 1.15, -1.98	0.03, 0.03, -0.07, 0.04, -0.08, 0.17
Nunatak	55.94	-148.9	3.74 ± 1.72	-31.31, -18.89, 54.09	134.02, 117.31, -301.97, 102.71, -264.35, 680.44
Foothills	34.79	-35.08	-0.48 ± 0.13	3.98, -4.82, -1.85	5.00, 4.36, -10.87, 3.84, -9.54, 23.79
E. Denali	65.15	-148.22	-0.30 ± 0.55	-1.14, 4.69, -2.13	12.99, 10.87, -30.42, 9.19, -25.59, 71.51

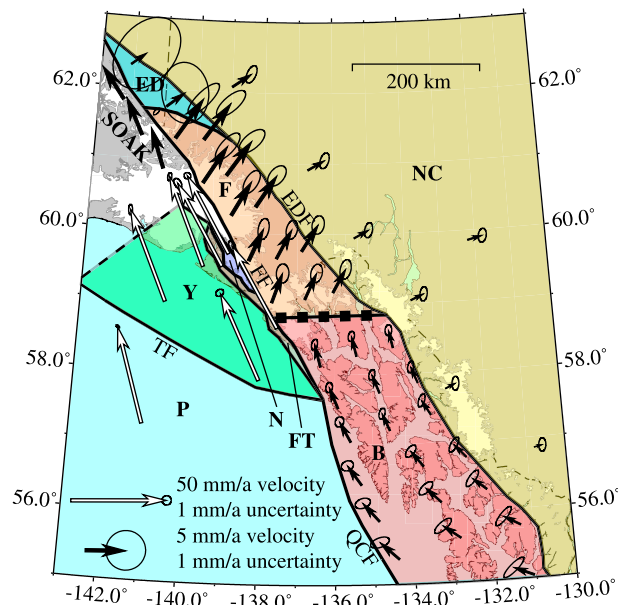


Figure 8. Block velocity predictions for selected points in southeast Alaska and adjacent Canada. Note the different vector scales used. All block velocity predictions are relative to the North America definition of *Sella et al.* [2007]. SOAK predictions are derived from *Fletcher* [2002]. Pacific plate velocity is derived from *Plattner et al.* [2007]. Abbreviations are P, Pacific plate; Y, Yakutat block; N, Nunatak block; FT, Foothills block; B, Baranof block; F, Fairweather block; NC, Northern Cordillera block; ED, Eastern Denali block; SOAK, Southern Alaska block; QCF, Queen Charlotte fault; FF, Fairweather fault; TF, Transition fault; EDF, Eastern Denali fault.

uncertainty in one component, typically the local vertical direction at the block in question. The nonlinear transformation between Cartesian and geographic coordinates means that the uncertainty regions for the Euler poles are distorted from ellipses into the shape of a great circle path when one axis of the Cartesian error ellipsoid is large. In addition, at the high latitudes considered in this study, a simple conversion of ellipse parameters can display a rotational bias in the error ellipse due to the difference scales (in distance units) of the latitude and longitude axes. For these reasons, we show a Monte Carlo sampling of the uncertainty regions instead of the usual 95% confidence ellipses with the poles in Figure 7. We took 2500 random samples of a distribution with zero mean and covariance equal to the angular velocity covariance, added each sample to our estimated angular velocities, computed the corresponding Euler pole, and plotted the pole as a point on the map. The density of the points on the map corresponds to the probability distribution of the pole location. For blocks with large uncertainty regions for the poles, the predicted linear block velocities for points on the blocks will still have small uncertainties. This results from the strong correlation between the pole location and the angular speed.

[48] We find the Yakutat block pole near the center of Hudson Bay in Canada, far from the block itself and consistent with the minimal rotation seen in the data along the northern coastal region of southeast Alaska. At the city of

Yakutat, our model predicts a block velocity of 50.3 ± 0.8 mm/a at an azimuth of $N22.9 \pm 0.6^\circ$ W (Figure 8). For comparison, the model of *Plattner et al.* [2007] predicts a Pacific plate velocity of 50.9 mm/a at an azimuth of $N14.6^\circ$ W at this location. Our estimate of the Yakutat block velocity is much closer to the velocity of the Pacific plate than the Yakutat estimate presented by *Fletcher and Freymueller* [1999], although a distinct difference in azimuth between the two tectonic blocks remains. At least part of the difference between the two geodetically derived estimates may be due to the fact that we removed the effects of GIA while the previous study did not. At YKTT, the Yakutat block GPS site used by *Fletcher and Freymueller* [1999], the predicted GIA motion is 3 mm/a, directed WSW. Removing this GIA estimate from the GPS data results in a more northerly directed velocity than that derived from the unadjusted data (Figure S2a).

[49] The Foothills block pole is the farthest away from southeast Alaska. Its location in the Atlantic Ocean results in block velocities that show little or no observable rotation along the block. This agrees well with the observed sub-parallel velocities on or near the Foothills block (Figure 4) and the linearity of the Fairweather fault in this region. Block velocity predictions display a similar magnitude but a more westerly azimuth than those for the Yakutat block.

[50] Unlike the poles discussed above, the pole for the Nunatak block is located to the west of our study area, south of the Alaska Peninsula. Predicted block velocities have smaller magnitudes but almost identical azimuths to those on the Foothills block. The Eastern Denali block pole is located north of the Denali fault. Counter-clockwise rotation about the pole results in N-NE directed block velocities that decrease in magnitude toward the north.

[51] The Northern Cordillera pole is located to the east of the Queen Charlotte Islands. While the azimuth of the block velocity predictions is uniformly NE in our study area, the magnitudes steadily decrease toward the south until the zero point is reached at the pole. The Fairweather and Baranof block poles are both found on the Northern Cordillera block, with the Baranof pole located east and north of the Fairweather pole. Velocities along the Fairweather block show variation in both magnitude and azimuth, with magnitudes decreasing from north to south and azimuths displaying a clockwise rotation. The Baranof block displays block velocities that are much smaller and more uniform in magnitude than those on the Fairweather block. The azimuths, however, show a distinct clockwise rotation.

5.2. Relative Block Motions

[52] Relative block motions resulting from our preferred model are shown in Figure 9. The majority of the relative motion between the Pacific plate and North America occurs along the Fairweather – Queen Charlotte system. Along the Fairweather fault, the motion is nearly pure translation while the Queen Charlotte fault displays varying degrees of transpression. Inboard of the Fairweather – Queen Charlotte system, the magnitude of the relative block motion remains fairly constant along the Eastern Denali and Coast Shear zone faults. The sense of motion, however, progresses from contraction and translation along the Eastern Denali fault to translation and dilatation along the Coast Shear Zone.

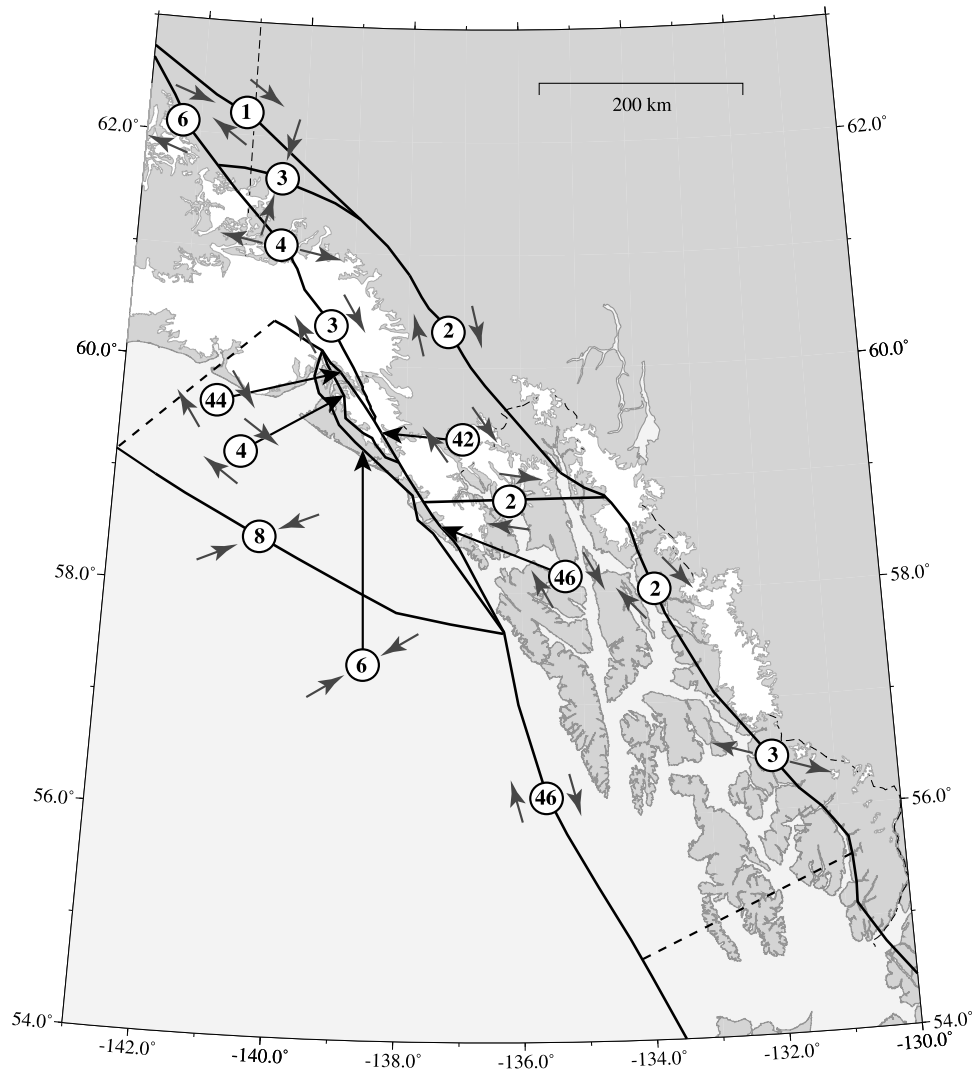


Figure 9. Relative block motion predictions for southeast Alaska. Dark gray arrows indicate sense of relative motion while the circled numbers give the magnitude of the motion in mm/a rounded to the nearest whole number. For faults with offset numbers, long black arrows connect the circled number to the appropriate fault.

The Duke River fault displays contraction between the Totschunda and Eastern Denali faults.

[53] Relative motion between the Pacific plate and the Yakutat block results in 7.9 ± 0.9 mm/a of oblique convergence across the Transition fault. Summed together, the Boundary and Foothills faults accommodate ~ 6 mm/a of relative convergence as well as ~ 4 mm/a of relative translation between the coast and the Fairweather fault.

[54] *Lahr and Plafker* [1980] suggested that relative block motion in this region may have recently begun shifting westward from the Duke River – Eastern Denali – Chatham Strait fault system to the Totschunda – Fairweather connector fault. Roughly double the amount of predicted relative block motion occurs on the Totschunda-Fairweather connector and Duke River faults than on the Eastern Denali and Coast Shear zone, so our results appear to support this idea.

[55] Overall, the relative block motion map provides a picture of the current influence of the Yakutat block on the

tectonics of southeast Alaska. In the northern part of the region, the complex combination of contraction, dilatation, and translation delineate the active collisional zone. Farther south, the relative motions indicate that the area has transformed from a collisional zone to a more translational boundary zone with some active deformation continuing inboard of the Queen Charlotte fault.

5.3. Goodness of Fit

[56] Our block model provides a reasonable explanation for the observed GPS velocity field in southeast Alaska and the adjacent region of Canada, as shown by the residual vector plot in Figure 10. The reduced χ^2 (χ^2 per degree of freedom) for our preferred model is 1.01, indicating that we have accounted for most of the effects of major structures and blocks in the region. 76% of the site-specific residual velocities are smaller than their $1-\sigma$ uncertainty estimates. The mean residual velocity magnitude is 1.1 mm/a while the

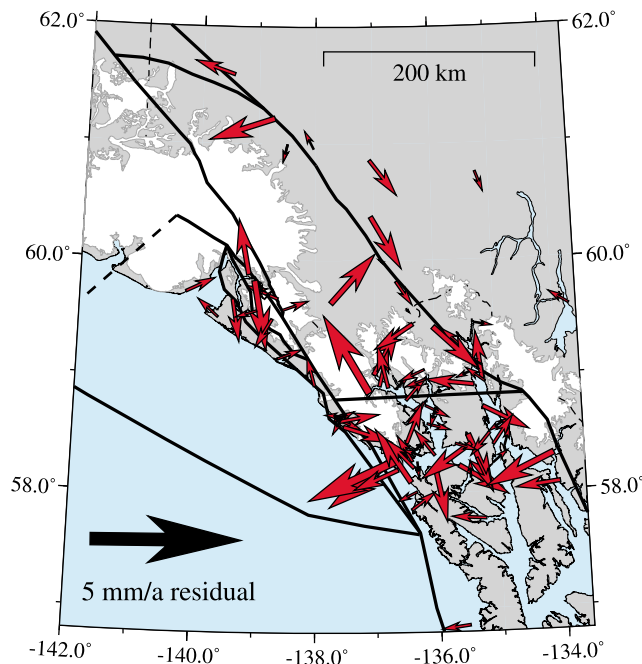


Figure 10. Velocity residuals between data and block model predictions. Residuals are only shown for sites whose data uncertainties are less than 1.5 times the average uncertainty. Using our preferred model, 76% of the sites have residuals smaller than their 1- σ uncertainty estimates.

mean data uncertainty magnitude is 1.7 mm/a. The residual velocities do not show a clear trend in any region.

6. Discussion

6.1. Slip Rate Estimates and Seismic Hazard

[57] The only two faults without slip constraints in our model that have previous geologic and geodetic slip estimates are the Fairweather fault and the Dalton strand of the Eastern Denali fault. *Plafker et al.* [1978] reported an average dextral slip rate of 48–58 mm/a over the past 1,000 years for the Fairweather fault based on geologic studies, but the dates used were imprecise. The lower end of that estimate is more likely since Pacific–North America relative plate motion is only about 50 mm/a in this area. Using EDM networks across the fault, *Lisowski et al.* [1987] estimated a slip rate of 41–51. The large range in this estimate results from a strong trade-off between slip rate and locking depth. *Fletcher and Freymueller* [2003] combined the GPS and EDM data to generate an estimate of about 46 mm/a.

[58] Our preferred block model gives an average slip rate of 42.9 ± 0.9 mm/a along the Fairweather fault. The slip rate estimate varies along strike, from 36.6 ± 0.8 mm/a along the northern end of the fault to 41.5 ± 0.8 mm/a along the central segment of the fault to 45.8 ± 1.2 mm/a near Cross Sound. At the average slip rate, it would take 80 years to recover the 3.5 m of slip that occurred during the 1958 Fairweather fault event. Within model uncertainties, the average slip rate given by our block model agrees with the geodetic estimate of *Fletcher and Freymueller* [2003].

[59] In their kinematic model, *Lahr and Plafker* [1980] proposed a dextral slip rate of 2 mm/a along the Eastern

Denali fault. Based on a combined profile of geodetic data across the Fairweather and Eastern Denali faults, *Fletcher and Freymueller* [2003] estimated that the Eastern Denali currently had a dextral slip rate of 3.8 mm/a. In these two studies, the region between the Fairweather and Eastern Denali faults moved northwestward roughly parallel to the Fairweather fault.

[60] Our block model predicts an average of 1.5 ± 0.5 mm/a of dextral slip and 1.5 ± 0.6 mm/a of contraction along the Dalton strand of the Eastern Denali fault. This slip estimate is lower and much more transpressional than the previous geodetic estimate. The difference results from our rotating Fairweather block, which gives nearly fault normal motion in the vicinity of the Eastern Denali fault, and our substitution of the rotating Northern Cordillera block for fixed North America.

[61] On the Boundary fault, our block model predicts an average of 3.6 ± 1.4 mm/a right-lateral strike-slip with an average 2.2 ± 1.5 mm/a of convergence across the northern end of the fault and 1.9 ± 1.2 mm/a of extension across the southern end of the fault. The change from convergence to extension occurs because of changes in the orientation of the model fault planes from north to south. Along the Foothills fault, our model predicts an average of 0.5 ± 1.6 mm/a of left-lateral strike-slip and 4.7 ± 0.9 mm/a of convergence. Slip estimates from our model are not directly comparable to the model of *Plafker and Thatcher* [2008] due to differences in fault geometry (see Section 4.2). Regardless of fault geometry differences, we can conclude that our GPS-constrained block model allows low to moderate amounts of strain accumulation in the area suspected of generating the 1899 earthquake sequence.

[62] Since it is offshore, direct measurements of the slip rate on the Queen Charlotte fault do not exist. In our block model, slip on the Queen Charlotte fault is defined by the relative motion between the Pacific plate and the Fairweather block. Our model predicts an average of 43.9 ± 0.6 mm/a fault parallel motion (right-lateral sense) and southward increasing convergence of 0.7 ± 0.4 mm/a (northern end of fault) to 15 ± 0.6 mm/a (north of the Queen Charlotte Islands). The increasing convergence is a result of the changing relative azimuth between the plate motion vectors and the model fault. At a rate of 43.9 mm/a, it would take about 130 years to recover the average slip of 5.8 m from the 1949 $M_w 8.1$ Queen Charlotte Island event reported by *Nishenko and Jacob* [1990].

[63] There is no consensus on slip rates and seismic hazard along the Transition fault among previously published estimates. *Fletcher and Freymueller* [2003] suggested that a freely slipping Transition fault could accommodate the ~ 20 mm/a of Fairweather fault normal motion implied by the GPS velocity at the city of Yakutat. In their model, the sense of slip on the Transition fault would be almost pure reverse motion. A suite of models presented by *Pavlis et al.* [2004] predicted 10 to 30 mm/a of dextral/oblique to pure convergent motion across the Transition fault. The kinematic model of *Lahr and Plafker* [1980] included 4 mm/a of dextral oblique motion across the Transition fault. Based on estimates of rupture length, focal depth, and moment of the 1973 main shock, *Doser and Lomas* [2000] calculated a convergent slip rate of ~ 3 mm/a over the last century for the segment of the Transition fault offshore of Cross Sound. Our

block model produces an average of 5.4 ± 1.1 mm/a of left-lateral strike-slip and 5.8 ± 0.9 mm/a of convergence across the Transition fault. Our fault normal estimate is quite close to those of both *Lahr and Plafker* [1980] and *Doser and Lomas* [2000], but it is substantially lower than the estimates of the previous model utilizing geodetic data. This difference is due to our inclusion of the Boundary and Foothills faults, which accommodate some of the relative convergence. The type of fault normal motion predicted by our model varies along the length of the Transition fault. We defined the northern and central sections of the fault as a vertical fault, so the fault normal estimate is represented by contraction. The southernmost section, around Cross Sound, was defined as a NE-dipping thrust fault, so the fault normal motion is translated into reverse slip.

6.2. Extent of Coherent Yakutat Block

[64] Some studies have suggested that structures within the Yakutat block such as the Dangerous River zone are currently active [e.g., *Gipp*, 2003] and thus create a block boundary running across the lower part of Yakutat Bay. Our results do not support this hypothesis. The GPS velocity field (Figure 4) shows nearly identical velocities at sites on the Yakutat block, suggesting that no active structure exists between them. All of the GPS data from sites on the Yakutat block can be explained by a combination of strain accumulation on nearby faults to the east and a block rotation described by a single pole and rotation rate. Based on these results, we conclude that the Yakutat block behaves as a coherent block from Cross Sound to at least the eastern side of the Malaspina Glacier.

[65] The eastern Yakutat block boundary in our model is the Foothills fault and is further west than the most oft-cited boundary, the Fairweather fault. GPS velocities between the coast and the Fairweather fault become progressively smaller and more westerly toward the east. This suggests that as the Yakutat block has jammed into the corner between the Pacific plate, southern Alaska, and western Canada, its eastern edge has undergone deformation and is now actively fragmenting. Such fragmentation would explain why the large earthquakes of the 1899 sequence occurred off of the major translational plate boundary formed by the Fairweather-Queen Charlotte system.

6.3. Significance of Nunatak and Foothills Blocks

[66] The Nunatak and Foothills blocks are the two smallest blocks in our model and their size raises questions about whether they can truly be called rigid blocks, whether our interpretation could be based on transient strain, and whether these blocks are actually required by our block model.

[67] The unlikelihood of detectable transient strain from the postseismic effects of the 1964, 1958, or 1899 earthquakes has been discussed in an earlier section. There remains the possibility that an under- or over-estimation of our predicted horizontal GIA effect could introduce a bias into the data, leading to spurious tectonic conclusions. To assess this possibility, we ran the alternate geometry model tests (see Section 4.2, Table 1, and Figure 6) using data sets that had had predictions from the two end-member GIA model predictions applied instead of those of our best fit model (see Section 3.4). Horizontal predictions from the two end-member GIA models differ substantially in both azimuth and

direction from our best fit GIA model (Figure S3), so the results from these tests should reveal any inherent bias. The results displayed no significant effects; the statistical conclusions were the same as those drawn from the best fit GIA model.

[68] The inclusion of the Foothills and Nunatak blocks improved the fit between the block model and the data in the northern Fairweather fault region to degrees that met or exceeded the *F* test criteria for significance at the 95% level (Table 1). Although this misfit reduction is important, it is the secondary reason for the inclusion of the blocks in our model. The main impetus is that without the two blocks, our model predicts ~ 20 mm/yr of contraction across the Transition fault. This amount of convergence would essentially place a subduction zone offshore southeast Alaska. As discussed earlier, offshore seismic data recently collected in the Gulf of Alaska (*G. Christeson*, personal communication, 2009) show no evidence for such a structure. Instead, the data suggest that the central section of the Transition fault is a near vertical structure.

[69] There remains the question of whether the Nunatak and Foothills blocks actually deserve the designation of "block." In the process of developing our block model, we found that the amount of convergence accommodated between the coastal region and the Fairweather fault was more important than the precise locations and geometries of the faults. To fit the GPS data, the northern half of the Boundary fault did require specific fault plane dips and locking depths. Along the southern half, the GPS data only required the presence of a creeping boundary (represented by a fault with a 0 km locking depth – Table 2). The Foothills fault was assigned a vertical geometry to minimize misfit and contraction across Transition fault, but a moderately NE-dipping geometry did not radically increase the misfit. Angular velocities for the Nunatak and Foothills blocks have large uncertainties (Table 3 and Figure 7) and are the most sensitive of all the blocks to changes in fault geometries.

[70] Given the complex nature of the Yakutat collisional corner, it is unlikely that the convergence is neatly or simply partitioned between the two faults presented here. Instead, the deformation could be distributed across the region on a number of structures whose exact geometries and slip rates are likely impossible to fully determine. Based on the evidence laid out in the previous paragraph, we propose that the Nunatak and Foothills blocks represent a deformation zone along the eastern edge of the Yakutat block rather than truly rigid blocks. Such a deformation zone would be realistic given the complicated tectonic environment of southeast Alaska and would accommodate the strain responsible for events like the 1899 earthquake sequence that occur off the main plate boundaries.

6.4. Transition Fault Paradox

[71] In our block model, the Transition fault accommodates oblique transpressive motion between the Pacific plate and the Yakutat block. The Transition fault is the obvious candidate for the Pacific-Yakutat boundary, but the amount and sense of present-day motion on the fault is controversial (see Section 2).

[72] Our block model predicts an average of 5.4 ± 1.1 mm/a of left-lateral strike-slip and 5.8 ± 0.9 mm/a of contraction along the Transition fault. This amount of predicted con-

vergence is far less than that suggested by *Fletcher and Freymueller* [1999], but more than might be expected in a dominantly strike-slip boundary. *Pavlis et al.* [2004] proposed that the rate of sedimentation in the Gulf of Alaska could mask evidence of convergence. Extremely high sedimentation rates of 10–30 mm/a have been reported for the region [e.g., *Jaeger et al.*, 1998; *Sheaf et al.*, 2003; *Hallet et al.*, 1996; *Koppes and Hallet*, 2002], implying that a substantial layer of sediment could accumulate over a relatively short time period. If our fairly modest amount of estimated convergence has been occurring over a comparably short time period, visible structures may not have developed yet. This could make our predicted motion along the Transition fault compatible with the available offshore seismic record.

[73] Another possibility is that the Pacific-Yakutat relative motion is divided between strike-slip on the Transition fault and motion on another fault. Between 1987 and 1992, a sequence of $M_w 7+$ earthquakes defined a north-south trending plane beginning near the junction of the Transition fault with the Pamplona zone and extending south into the Pacific plate [*Lahr et al.*, 1988; *Pegler and Das*, 1996]. The fault plane coincided with a preexisting weakness in the Pacific plate, magnetic anomaly 13. The two largest events of the sequence had right-lateral strike-slip mechanisms. Seismic reflection lines in the Gulf of Alaska [*Reece et al.*, 2009] suggest the presence of an active zone of faulting coincident with the north-south trending plane (Figure 1). The lack of offshore GPS sites or other constraints prevents us from including a Gulf of Alaska fault in our block model inversion. We can, however, estimate the slip rates on the a Gulf of Alaska fault and the Transition fault required to completely accommodate the Pacific-Yakutat relative motion through a simple linear combination solution. Assuming pure strike-slip motion on both faults and our predicted relative motion of 7.4 ± 1 mm/a east and 2.8 ± 1 mm/a north, we obtain estimates of 8.3 ± 1.0 mm/a of left-lateral slip on the Transition fault and 6.5 ± 1.1 mm/a of right-lateral slip on the Gulf of Alaska fault. The combination of left-lateral slip on the Transition fault and right-lateral slip on the Gulf of Alaska fault would require internal deformation of the block located between the two faults. A simple rotation of the block is not adequate.

[74] The currently available data do not allow us to unequivocally confirm or disallow the sedimentation hypothesis, slip rates on a Gulf of Alaska fault and the Transition fault, or the amount of internal deformation between the two faults. But taken together, the sedimentation hypothesis and the Gulf of Alaska/Transition fault combination form reasonable end-member solutions to the problem of reconciling our predicted Pacific-Yakutat relative motion and the offshore seismic data.

6.5. Glacier Bay Structures

[75] Our block model includes a boundary running through Tidal Inlet in Glacier Bay, dividing the Fairweather and Baranof blocks. We chose the location of this boundary, which we termed the Glacier Bay Partition (GBP), based on seismicity patterns and geologic observations of structural trends. The inclusion of the GBP improved the overall reduced χ^2 by $\sim 10\%$ and exceeded the F test criteria for significance at the 99% level (Table 1).

[76] Given that Glacier Bay is the current focus of considerable GIA effects due to ice loss since the LIA, there is a possibility that the signal we interpret as tectonic deformation could be an artifact introduced by our use of our best fit GIA model. To test the dependence of our Glacier Bay conclusion on the GIA model predictions, we ran versions of our block inversion with and without the GBP using data that had the predictions of the two end-member GIA models (see Section 3.4) applied instead of the best fit model. For the case of the 50 km, 7×10^{18} Pa s GIA model, the version with the GBP had a reduced χ^2 value over 10% smaller than the version without and exceeded the F test criteria for significance at the 99% level. In the case of the 85 km, 1.5×10^{18} Pa s GIA model, the version with the GBP had a reduced χ^2 value about 5% smaller than the version without and met the F test criteria for significance at the 98% level. The relative independence of our GBP results from the choice of GIA models is not an unexpected result; while vertical GIA effects reach some of their maximum values in the Glacier Bay area, horizontal GIA effects are quite small there (Figures S2b and 3).

[77] There remains the question of whether the GBP represents an actual discrete structure or if it instead serves as a proxy for distributed deformation. Our block model predicts 1.5 ± 0.4 mm/a of dextral slip and negligible fault-normal motion on the GBP. The Fairweather and Baranof block angular velocities predict very similar motions on their block boundary, but quite different motions away from the boundary. The available earthquake focal mechanisms do not show evidence of right-lateral strike-slip motion but instead indicate mixed strike-slip/thrust events. We found that the exact orientation of the Glacier Bay Partition was not crucial to the model results. Faults oriented 10° , 20° , and 30° from our model fault (Figure 5) did not cause significant changes in the misfit.

[78] Based on these findings, we propose that the GBP represents internal deformation of the region comprising our Fairweather and Baranof blocks. The deformation north of Glacier Bay (Fairweather block) is strongly influenced by its proximity to the active collisional front between the Yakutat block and southern Alaska. Strain transferred from the collision is forcing the Fairweather block to move to the northeast. The magnitude of the block velocities and their degree of easterly rotation decreases toward the south as distance from the collisional front in the St. Elias mountains increases (Figures 1 and 8). South of the GBP, block velocity magnitudes along the Baranof block are much smaller and more uniform than those observed to the north, but a distinct clockwise rotation is still evident. The rotation may be a result of the Baranof block being pulled along with the Fairweather block as the latter is pushed northeastward. The difference in deformation north and south of the GBP provides an explanation for the dearth of seismicity along the Chatham Strait fault and in the rest of the Baranof block (Figure 2) as well as the southward decreasing magnitudes in the GPS data and block motion predictions along the Northern Cordillera block.

6.6. Southern Boundary of the Baranof Block

[79] Our block model does not define a unique southern boundary for the Baranof block. Our data set is very sparse

south of 58°N and includes no sites south of 55°N, so the model does not have adequate constraints in this region to exactly determine the boundary. We can, however, indirectly constrain the limits of the Baranof block.

[80] *Mazzotti et al.* [2003] noted that the GPS velocities at sites in the Queen Charlotte Islands (Figure 1) had a significant margin-normal component. They found that the GPS data, in particular the margin-normal component, could not be explained by elastic deformation from the Queen Charlotte fault, even if a landward-dipping thrust was assumed to be part of the offshore plate boundary. This led them to suggest that the GPS data required active faulting between the Queen Charlotte Islands and stable North America. We repeated their experiment, with the Baranof block in place of North America, to test whether the Queen Charlotte Islands lie on the Baranof block or whether the Baranof block motion modifies their conclusion. Our results were similar to those of *Mazzotti et al.* [2003] – the GPS velocities in the Queen Charlotte Islands could not be fully explained by a landward-dipping thrust fault accommodating the margin-normal component of the Pacific-Baranof block relative motion. This suggests that the Queen Charlotte Islands move independently of both North America and the Baranof block. Thus the Queen Charlotte Islands represent a different tectonic regime than the region to the north, likely due to the high degree of transpression along the offshore plate boundary. This conclusion agrees with the results of *Leonard et al.* [2008] and *Mazzotti et al.* [2008], who proposed that a coastal block including the Queen Charlotte Islands moves northerly at a rate of ~ 5 mm/a. In comparison, our model predicts ~ 4 mm/a of WSW-directed motion for the Baranof block in the Queen Charlotte Island region.

[81] In the course of the above test, we found that one of the GPS sites in our southeast Alaska data set likely belongs in the Queen Charlotte tectonic regime. After removing the elastic signal predicted by the fault model discussed above, the residual at this site (AIS1 on Annette Island, Figure 1) closely resembled the residuals seen at sites in the Queen Charlotte Islands. Based on this, we excluded AIS1 from our modeling and conclude that the Baranof block ends north of Annette Island (see dashed line in Figure 5).

6.7. Northern Cordillera Block and Strain Transfer

[82] As Figures 4 and S4 show, the GPS velocities at sites on the Northern Cordillera block are small, especially toward the south. This raises the question of whether the Northern Cordillera block actually has distinct motion or is just part of the North American plate. The definition of the Northern Cordillera block is primarily based on GPS data, following *Mazzotti and Hyndman* [2002] who noted that a continuous GPS station at Whitehorse in the northern Canadian Cordillera showed about 5 mm/a of northeastward motion relative to North America. They suggested that the northeastward motion of the northern Cordillera block was due to strain transfer from the Yakutat block collision. Using a larger set of GPS sites, *Leonard et al.* [2008] documented a pattern of northeastward motion east of the Eastern Denali fault. Magnitudes of the velocities decreased from north to south. Our velocity field shows a similar pattern (Figure 4). As mentioned earlier, we see a decrease in velocity magnitude from ~ 6 mm/a north of the Duke River fault to less than 1 mm/a

in the southeast of Chatham Strait. Previous studies [e.g., *Mazzotti and Hyndman*, 2002; *Leonard et al.*, 2008; *Mazzotti et al.*, 2008] have discussed the seismicity in the Richardson and Mackenzie Mountains to the north and northeast of our study area, which strongly suggests that the Northern Cordillera is moving northeasterly relative to stable North America.

[83] We tested a block model with North America substituted for the Northern Cordillera to determine the importance of the latter block. Defining the region east of the Eastern Denali and Coast Shear Zone faults to be North America increased overall misfit between the GPS data and our block model by about 15%, with the largest residuals concentrated near or east of the Eastern Denali fault. Several sites, including WHIT, a well-established continuous GPS station, had residuals approaching the $2\text{-}\sigma$ level. When compared to the North America version, the Northern Cordillera block model had an F value of 9.6, which exceeds the F test criteria for significance at the 99% level. These results strongly suggest that the Northern Cordillera has a motion distinct from that of stable North America.

[84] Small velocities such as the ones seen in the Northern Cordillera might be caused by transient strain instead of long-term tectonic block motion. A possible source of transient signal could be a under- or over-estimation of the horizontal GIA effects in southeast Alaska. To test this possibility, we ran the test discussed in the previous paragraph using data that had had the two end-member GIA models applied instead of our best fit model. In both cases, the block model version including the Northern Cordillera block had an overall misfit more than 10% smaller than the North America version and exceeded the F test criteria for significance at the 99% level. Another likely candidate for non-tectonic transient motion would be GIA from the loss of the Laurentide Ice Sheet. The ICE4G model [*Peltier*, 2002] estimates that the horizontal motion from GIA effect in the Northern Cordillera would be small (< 2 mm/a) and oriented W-SW. Removing this signal would intensify the N-NE trend seen in the GPS velocities, not diminish it. Strain accumulation on an unrecognized locked fault is also not a probable explanation. There are simply no candidate faults that could produce N-NE-directed deformation over such a large area.

[85] The eastern and southern boundaries of the Northern Cordillera block are not clearly delineated and our data set does not extend far enough to directly examine the possible alternatives. *Leonard et al.* [2008] found that GPS velocities at sites located east of the Mackenzie and Canadian Rocky Mountains displayed near-zero horizontal motion, suggesting that they represent stable North America. To the south, *McCaffrey et al.* [2007] presented a block model for the western Cordillera that included several blocks in southwestern British Columbia. We compared predicted block velocities from our Northern Cordillera block to the predicted velocities of the British Columbia blocks to see if they were compatible. The Northern Cordillera block predictions were larger and oriented in the opposite direction than the British Columbia block predictions. Based on this, we conclude that the Northern Cordillera block terminates north of this region.

[86] An unresolved problem is how strain is transferred from the main plate boundary zone into the Northern Cordillera. Based on high heat flow measurements, *Mazzotti and Hyndman* [2002] devised a model for the Cordillera that

involves a strong upper crust over a hot, weak, lower crust. This weak lower crust could serve as a detachment and allow the upper crust to move over the uppermost mantle. In this model, a small amount of Yakutat–North America relative motion is transferred into the Cordilleran upper crust, which then moves as a semi-rigid block over the weak lower crust and eventually thrusts over the stable craton. Such a model would allow the translation of the upper crust without much internal deformation.

[87] In our block model, a portion of the Yakutat–North America relative motion is transmitted directly from the main plate boundary zone into the Fairweather and Baranof blocks, which then undergo clearly defined rotations. East of the Fairweather and Baranof blocks, our Northern Cordillera results are completely compatible with the model of *Mazzotti and Hyndman* [2002]. However, from our modeling we cannot rule out the alternative possibility that the Northern Cordillera is a rigid block and that the convergence at its eastern boundary involves slip on faults that cut through the lithosphere.

7. Conclusions

[88] We have used an extensive GPS data set to develop a block model for southeastern Alaska and the adjoining region of Canada. The block model provides an integrated kinematic view of the regional tectonics and provides new constraints on seismic hazard evaluation.

[89] Southeast Alaska is strongly affected by the collision of the Yakutat block with southern Alaska and our block model provides a snapshot of the present tectonic response. According to our model, the Yakutat block is moving at a velocity of 50.3 ± 0.8 mm/a toward $N22.9 \pm 0.6^\circ$ W, a velocity that is similar in magnitude but more westerly than the velocity of the Pacific plate. The relative block motion between the Yakutat block and the Southern Alaska block indicates that ~ 45 mm/a of convergence must be accommodated across the St. Elias orogen to the north of our study area. The eastern edge of the Yakutat block is deforming, represented in the model by two small northwesterly moving blocks located west of the Fairweather fault. Part of the strain from the collision is transferred east of the Fairweather – Queen Charlotte system and causes the area north of Glacier Bay to rotate clockwise into the Northern Cordillera. The region south of Glacier Bay undergoes a much slower clockwise rotation and may be at least partially pulled along by the northern block motion. Strain is also transferred further east into the Northern Cordillera block, which displays small northeasterly motions. Our results suggest that the entire southeastern Alaska margin is mobile.

[90] The vast majority of the relative block motion (and thus most of the seismic hazard) is concentrated along the Fairweather–Queen Charlotte fault system. Our block model predicts average dextral slip of 42.9 ± 0.9 mm/a along the Fairweather fault and transpressive relative motion along the Queen Charlotte fault equivalent to 43.8 ± 0.6 mm/a. In our model, combination of dextral and reverse slip on the Boundary and Foothills faults accommodates about half of the observed convergence between the Pacific plate and the Fairweather fault. A deformation zone encompassing these two faults could provide an explanation for the 1899 Yakutat Bay earthquakes. The remaining relative motion is taken up

on an offshore fault, here taken to be the Transition fault. GPS velocities along the coastal regions cannot be explained without the presence of the offshore fault.

[91] **Acknowledgments.** Thora Árnadóttir and two anonymous reviewers provided helpful comments. We thank Stéphane Mazzotti and Lucinda Leonard for providing data from sites in the Canadian Cordillera and the Queen Charlotte Islands. We also thank Natasha Ruppert for providing focal mechanism information and comments about seismicity patterns, Peter Hauessler for providing geologic slip rate estimates on the northern Eastern Denali fault, and Wes Wallace for helpful discussions. Glacier Bay National Park provided assistance with remote field logistics. Figures were generated with the Generic Mapping Tools software of *Wessel and Smith* [1998]. This research was funded by NSF grants EAR-0409426, EAR-0408801, EAR-0229934, and EAR-9870144.

References

- Arendt, A. A., K. A. Echelmeyer, W. D. Harrison, C. S. Lingle, and V. B. Valentine (2002), Rapid wastage of Alaska glaciers and their contribution to rising sea level, *Science*, **297**, 382–386, doi:10.1126/science.1072497.
- Argus, D. F. (2007), Defining the translational velocity of the reference frame of Earth, *Geophys. J. Int.*, **169**, 830–838, doi:10.1111/j.1365-246X.2007.03344.x.
- Árnadóttir, T., B. Lund, W. Jiang, H. Geirsson, H. Björnsson, P. Einarsson, and T. Sigurdsson (2009), Glacial rebound and plate spreading: Results from the first countrywide GPS observations in Iceland, *Geophys. J. Int.*, **177**, 691–716.
- Brew, D. A. (1994), Latest Mesozoic and Cenozoic magmatism in southeastern Alaska, in *The Geology of North America*, vol. G1, *The Geology of Alaska*, edited by G. Plafker and H.C. Berg, pp. 621–656, Geol. Soc. Am., Boulder, Colo.
- Brew, D. A., and A. B. Ford (1981), The Coast plutonic complex sill, southeastern Alaska, in *The U.S. Geological Survey in Alaska: Accomplishments During 1978*, edited by N. R. D. Albert and T. L. Hudson, *U.S. Geol. Surv. Circ.* **823-B**, B96–B98.
- Brew, D. A., and A. B. Ford (1998), The Coast Mountains shear zones in southeastern Alaska—Descriptions, relations, and lithologic terrance significance, in *Geologic Studies in Alaska by the U.S. Geological Survey, 1996*, edited by J. E. Gray and J. R. Riehle, *U.S. Geol. Surv. Prof. Pap.*, **1595**, 183–192.
- Brew, D. A., B. R. Johnson, D. Grybeck, A. Griscon, D. F. Barnes, A. L. Kimball, J. C. Still, and J. L. Rataj (1978), Mineral Resources of Glacier Bay National Monument Wilderness Study Area, Alaska, *U.S. Geol. Surv. Open File Rep.*, **78-494**, 712 pp.
- Bruns, T. R. (1983), Model for the origin of the Yakutat Block, an accreting terrane in the northern Gulf of Alaska, *Geology*, **11**, 718–721, doi:10.1130/0091-7613(1983)11<718:MFTOOT>2.0.CO;2.
- Clague, J. J., and S. G. Evans (1993), Historic retreat of Grand Pacific and Melbern Glaciers, St. Elias Mountains, Canada: An analogue for decay of the Cordilleran ice sheet at the end of the Pliocene?, *J. Glaciol.*, **39**, 619–624.
- Doig, R. (1998), Paleoseismological evidence from lake sediments for recent movement on the Denali and other faults, Yukon Territory, Canada, *Tectonophysics*, **296**, 363–370, doi:10.1016/S0040-1951(98)00152-8.
- Doser, D. I. (2006), Relocations of earthquakes (1899–1917) in south-central Alaska, *Pure Appl. Geophys.*, **163**, 1461–1476, doi:10.1007/s00024-006-0085-3.
- Doser, D. I., and R. Lomas (2000), The transition from strike-slip to oblique subduction in southeastern Alaska from seismological studies, *Tectonophysics*, **316**, 45–65, doi:10.1016/S0040-1951(99)00254-1.
- Dziwonski, A. M., and D. L. Anderson (1981), Preliminary Reference Earth Model (PREM), *Phys. Earth Planet. Inter.*, **25**, 297–356, doi:10.1016/0031-9201(81)90046-7.
- Ferris, A., G. A. Abers, D. H. Christensen, and E. Veenstra (2003), High resolution image of the subducted Pacific (?) Plate beneath central Alaska, 50–150 km depth, *Earth Planet. Sci. Lett.*, **214**, 575–588, doi:10.1016/S0012-821X(03)00403-5.
- Fletcher, H. (2002), Crustal deformation in Alaska measured using Global Positioning System, Ph.D. dissertation, 135 pp., Univ. of Alaska Fairbanks, Fairbanks.
- Fletcher, H. J., and J. T. Freymueller (1999), New constraints on the motion of the Yakutat Block, *Geophys. Res. Lett.*, **26**, 3029–3032, doi:10.1029/1999GL005346.
- Fletcher, H. J., and J. T. Freymueller (2003), New constraints on the motion of the Fairweather Fault, Alaska, from GPS observations, *Geophys. Res. Lett.*, **30**(3), 1139, doi:10.1029/2002GL016476.

- Freed, A. M., R. Burgmann, E. Calais, J. Freymueller, and S. Hreinsdóttir (2006), Implications of deformation following the 2002 Denali, Alaska, earthquake for postseismic relaxation processes and lithospheric rheology, *J. Geophys. Res.*, **111**, B01401, doi:10.1029/2005JB003894.
- Freymueller, J. T., S. C. Cohen, R. Cross, J. Elliott, H. Fletcher, C. Larsen, S. Hreinsdóttir, and C. Zweck (2008), Active deformation processes in Alaska, based on 15 years of GPS measurements, in *Active Tectonics and Seismic Potential of Alaska*, edited by J. T. Freymueller et al., pp. 1–42, AGU, Washington, D. C.
- Gipp, M. R. (2003), Subsidence and tectonic controls on glacially influenced continental margins: Examples from the Gulf of Alaska and the western Scotian Shelf and Slope, *Quat. Int.*, **99–100**, 3–27, doi:10.1016/S1040-6182(02)00109-X.
- Gulick, S. P. S., L. A. Lowe, T. L. Pavlis, J. V. Gardner, and L. A. Mayer (2007), Geophysical insights into the Transition Fault debate: Propagating strike-slip in response to stalling Yakutat Block subduction in the Gulf of Alaska, *Geology*, **35**, 763–766, doi:10.1130/G23585A.1.
- Hallet, B., L. Hunter, and J. Bogen (1996), Rates of erosion and sediment evacuation by glaciers: A review of field data and their implications, *Global Planet. Change*, **12**, 213–235.
- Harrison, W. D., C. F. Raymond, K. A. Echelmeyer, and R. M. Krimmel (2003), A macroscopic approach to glacier dynamics, *J. Glaciol.*, **49**, 13–21, doi:10.3189/172756503781830917.
- Henton, J. A., M. R. Craymer, R. Ferland, H. Dragert, S. Mazzotti, and D. L. Forbes (2006), Crustal motion and deformation monitoring of the Canadian landmass, *Geomatica*, **60**, 173–191.
- Horner, R. B. (1983), Seismicity in the St. Elias region of northwestern Canada and southeastern Alaska, *Bull. Seismol. Soc. Am.*, **73**, 1117–1137.
- Hreinsdóttir, S., J. T. Freymueller, R. Bürgmann, and J. Mitchell (2006), Cosismic deformation of the 2002 Denali fault earthquake: Insights from GPS measurements, *J. Geophys. Res.*, **111**, B03308, doi:10.1029/2005JB003676.
- Jaeger, J. M., C. A. Nittrouer, N. D. Scott, and J. D. Milliman (1998), Sediment accumulation along a glacially impacted mountainous coastline: Northeast Gulf of Alaska, *Basin Res.*, **10**, 155–173.
- Johnson, K. M., R. Bürgmann, and J. T. Freymueller (2009), Coupled afterslip and visco-elastic flow following the 2002 Denali fault, Alaska earthquake, *Geophys. J. Int.*, **176**, 670–682, doi:10.1111/j.1365-246X.2008.04029.x.
- Kalbas, J. L., A. M. Freed, and K. D. Ridgway (2008), Contemporary fault mechanics in southern Alaska, in *Active Tectonics and Seismic Potential of Alaska*, edited by J. T. Freymueller et al., pp. 321–336, AGU, Washington, D. C.
- Klepeis, K. A., M. L. Crawford, and G. Gehrels (1998), Structural history of the crustal-scale Coast shear zone north of Portland Canal, southeast Alaska and British Columbia, *J. Struct. Geol.*, **20**(7), 883–904, doi:10.1016/S0191-8141(98)00020-0.
- Kogan, M. G., and G. M. Steblov (2008), Current global plate kinematics from GPS (1995–2007) with the plate-consistent reference frame, *J. Geophys. Res.*, **113**, B04416, doi:10.1029/2007JB005353.
- Koppes, M. N., and B. Hallet (2002), Influence of rapid glacial retreat on the rate of erosion by tidewater glaciers, *Geology*, **30**, 47–50.
- Lagoe, M. B., C. H. Eyles, N. Eyles, and C. Hale (1993), Timing of late Cenozoic tidewater glaciation in the far North Pacific, *Geol. Soc. Am. Bull.*, **105**, 1542–1560, doi:10.1130/0016-7606(1993)105<1542:TOLCTG>2.3.CO;2.
- Lahr, J. C., and G. Plafker (1980), Holocene Pacific-North American plate interaction in southern Alaska: Implications for the Yakutat seismic gap, *Geology*, **8**, 483–486, doi:10.1130/0091-7613(1980)8<483:HPAPII>2.0.CO;2.
- Lahr, J. C., R. A. Page, C. D. Stephens, and D. H. Christensen (1988), Unusual earthquakes in the Gulf of Alaska and fragmentation of the Pacific Plate, *Geophys. Res. Lett.*, **15**, 1483–1486.
- Lanphere, M. A. (1978), Displacement history of the Denali fault system, Alaska and Canada, *Can. J. Earth Sci.*, **15**, 817–822.
- Larsen, C. F., R. J. Motyka, J. T. Freymueller, K. A. Echelmeyer, and E. R. Ivins (2004), Rapid uplift of southern Alaska caused by recent ice loss, *Geophys. J. Int.*, **158**, 1118–1133, doi:10.1111/j.1365-246X.2004.02356.x.
- Larsen, C. F., R. J. Motyka, J. T. Freymueller, K. A. Echelmeyer, and E. R. Ivins (2005), Rapid viscoelastic uplift in southeast Alaska caused by post-Little Ice Age glacial retreat, *Earth Planet. Sci. Lett.*, **237**, 548–560, doi:10.1016/j.epsl.2005.06.032.
- Leonard, L. J., R. D. Hyndman, S. Mazzotti, L. Nikolaishen, M. Schmidt, and S. Hippchen (2007), Current deformation in the northern Canadian Cordillera inferred from GPS measurements, *J. Geophys. Res.*, **112**, B11401, doi:10.1029/2007JB005061.
- Leonard, L. J., S. Mazzotti, and R. D. Hyndman (2008), Deformation rates estimated from earthquakes in the northern Cordillera of Canada and eastern Alaska, *J. Geophys. Res.*, **113**, B08406, doi:10.1029/2007JB005456.
- Lisowski, M., J. C. Savage, and R. O. Buford (1987), Strain accumulation across the Fairweather and Totschunda faults, Alaska, *J. Geophys. Res.*, **92**, 11,552–11,560, doi:10.1029/JB092iB11p11552.
- MacKevett, E. M., D. A. Brew, C. C. Hawley, L. C. Huff, and J. G. Smith (1971), Mineral resources of Glacier Bay National Monument, Alaska, *U.S. Geol. Surv. Prof. Pap.*, **632**, 96 pp.
- Mazzotti, S., and R. D. Hyndman (2002), Yakutat collision and strain transfer across the northern Canadian Cordillera, *Geology*, **30**, 495–498, doi:10.1130/0091-7613(2002)030<0495:YCASTA>2.0.CO;2.
- Mazzotti, S., R. D. Hyndman, P. Flück, A. J. Smith, and M. Schmidt (2003), Distribution of the Pacific/North America motion in the Queen Charlotte Islands–S. Alaska plate boundary zone, *Geophys. Res. Lett.*, **30**(14), 1762, doi:10.1029/2003GL017586.
- Mazzotti, S., L. J. Leonard, R. D. Hyndman, and J. F. Cassidy (2008), Tectonics, dynamics, and seismic hazard in the Canada-Alaska Cordillera, in *Active Tectonics and Seismic Potential of Alaska*, edited by J. T. Freymueller et al., pp. 297–320, AGU, Washington, D. C.
- McCaffrey, R. (2002), Crustal block rotations and plate coupling, in *Plate Boundary Zones*, edited by S. Stein and J. Freymueller, pp. 101–122, AGU, Washington, D. C.
- McCaffrey, R., A. I. Kumar, R. W. King, R. Wells, G. Khazaradze, C. A. Williams, C. W. Stevens, J. J. Vollick, and P. C. Zwick (2007), Fault locking, block rotation and crustal deformation in the Pacific Northwest, *Geophys. J. Int.*, **169**, 1315–1340, doi:10.1111/j.1365-246X.2007.03371.x.
- McClelland, W. C., G. E. Gehrels, S. D. Samson, and P. J. Patchett (1992), Structural and geochronologic relations along the western flank of the Coast Mountains Batholith: Stikine River to Cape Fanshaw, central southeastern Alaska, *J. Struct. Geol.*, **10**(4), 107–123.
- McClelland, W. C., B. Tikoff, and C. A. Manduca (2000), Two-phase evolution of accretionary margins: Examples from the North American Cordillera, *Tectonophysics*, **326**, 37–55, doi:10.1016/S0040-1951(00)00145-1.
- Meade, B. J., and B. H. Hager (1999), Simultaneous inversions of geodetic and geologic data for block motions in plate boundary zones, *Eos Trans. AGU*, **80**(46), Fall Meet. Suppl., F267–F268.
- Meade, B. J., and B. H. Hager (2005), Block models of crustal motion in southern California constrained by GPS measurements, *J. Geophys. Res.*, **110**, B03403, doi:10.1029/2004JB003209.
- Meade, B. J., B. H. Hager, S. C. McClusky, R. E. Rellinger, S. Ergintav, O. Lenk, A. Barka, and H. Ozener (2002), Estimates of seismic potential in the Marmara Sea region from block models of secular deformation constrained by Global Positioning System measurements, *Bull. Seismol. Soc. Am.*, **92**, 208–215, doi:10.1785/0120000837.
- Milne, G. A., J. L. Davis, J. X. Mitrovica, H.-G. Scherneck, J. M. Johansson, M. Vermeer, and H. Koivula (2001), Space-geodetic constraints on glacial isostatic adjustment in Fennoscandia, *Science*, **291**, 2381–2385, doi:10.1126/science.1057022.
- Motyka, R. J. (2003), Little ice age subsidence and post little ice age uplift at Juneau, Alaska inferred from dendrochronology and geomorphology, *Quat. Res.*, **59**, 300–309, doi:10.1016/S0033-5894(03)00032-2.
- Nishenko, S. P., and K. H. Jacob (1990), Seismic potential of the Queen Charlotte-Alaska-Aleutian seismic zone, *J. Geophys. Res.*, **95**, 2511–2532, doi:10.1029/JB095iB03p02511.
- Okada, Y. (1985), Surface deformation due to shear and tensile faults in a half-space, *Bull. Seismol. Soc. Am.*, **75**, 1135–1154.
- Pavlis, T. L., C. Picornell, L. Serpa, R. L. Bruhn, and G. Plafker (2004), Tectonic processes during oblique collision: Insights from the St. Elias orogen, northern North American Cordillera, *Tectonics*, **23**, TC3001, doi:10.1029/2003TC001557.
- Pegler, G., and S. Das (1996), The 1987–1992 Gulf of Alaska earthquakes, *Tectonophysics*, **257**, 111–136.
- Peltier, W. R. (2002), Global glacial isostatic adjustment: Palaeogeodetic and space-geodetic tests of the ICE-4G (VM2) model, *J. Quat. Sci.*, **17**, 491–510, doi:10.1002/jqs.713.
- Perez, O. J., and K. H. Jacob (1980), Tectonic model and seismic potential of the eastern Gulf of Alaska and Yakutat Seismic Gap, *J. Geophys. Res.*, **85**, 7132–7150, doi:10.1029/JB085iB12p07132.
- Plafker, G., and W. Thatcher (2008), Geological and geophysical evaluation of the mechanism of the great 1899 Yakutat Bay Earthquake, in *Active Tectonics and Seismic Potential of Alaska*, edited by J. T. Freymueller et al., pp. 215–236, AGU, Washington, D. C.
- Plafker, G., J. C. Moore, and G. R. Winkler (1994a), Geology of the southern Alaska margin, in *The Geology of North America*, vol. G1, *The Geology of Alaska*, edited by G. Plafker and H. C. Berg, pp. 389–449, Geol. Soc. Am., Boulder, Colo.
- Plafker, G., L. Gilpin, and J. Lahr (1994b), Neotectonic map of Alaska, in *The Geology of North America, Decade of North American Geology*,

- vol. G-1, edited by G. Plafker and H. C. Berg, plate 12, Geol. Soc. Am., Boulder, Colo.
- Plafker, G., T. Hudson, T. R. Bruns, and M. Rubin (1978), Late Quaternary offsets along the Fairweather faults and crustal plate interactions in southern Alaska, *Can. J. Earth Sci.*, **15**, 805–816.
- Plattner, C., R. Malservisi, T. H. Dixon, P. LaFemina, G. F. Sella, J. Fletcher and F. Suarez-Vidal (2007), New constraints on relative motion between the Pacific Plate and Baja California microplate (Mexico) from GPS measurements, *Geophys. J. Int.*, **170**, 1373–1380, doi:10.1111/j.1365-246X.2007.03494.x.
- Pollitz, F. F. (2005), Transient rheology of the upper mantle beneath central Alaska inferred from the crustal velocity field following the 2002 Denali earthquake, *J. Geophys. Res.*, **110**, B08407, doi:10.1029/2005JB003672.
- Porter, S. C. (1989), Late Holocene fluctuations of the fiord glacier system in Icy Bay, Alaska, *Arct. Alp. Res.*, **21**, 364–379, doi:10.2307/1551646.
- Reece, R., S. P. Gulick, G. L. Christeson, and L. L. Worthington (2009), Intraplate shearing and basin deformation in the Pacific Plate as a result of the Yakutat Block collision with North America, *Eos Trans. AGU*, **90**(52), Fall Meet. Suppl., Abstract T33C–1924.
- Richter, D. H., and N. A. Matson (1971), Quaternary faulting in the eastern Alaska Range, *Geol. Soc. Am. Bull.*, **82**, 1529–1540.
- Rusmore, M. E., G. Gehrels, and G. J. Woodsworth (2001), Southern continuation of the Coast shear zone and Paleocene strain partitioning in British Columbia–southeast Alaska, *Geol. Soc. Am. Bull.*, **113**, 961–975.
- Schell, M. M., and L. J. Ruff (1989), Rupture of a seismic gap in southeastern Alaska: The Sitka earthquake (Ms 7.6), *Phys. Earth Planet. Inter.*, **54**, 241–257, doi:10.1016/0031-9201(89)90246-X.
- Seitz, G. J., P. J. Haeussler, A. J. Crone, P. Lipovsky, and D. P. Schwartz (2008), Eastern Denali fault slip rate and paleoseismic history, Kluane Lake area Yukon Territory, Canada, *Eos Trans. AGU*, **89**(53), Fall Meet. Suppl., Abstract T53B–1947.
- Sella, G. F., S. Stein, T. H. Dixon, M. Craymer, T. S. James, S. Mazzotti, and R. K. Dokka (2007), Observation of glacial isostatic adjustment in “stable” North America with GPS, *Geophys. Res. Lett.*, **34**, L02306, doi:10.1029/2006GL027081.
- Sheaf, M. A., L. Serpa, and T. L. Pavlis (2003), Exhumation rates in the St. Elias Mountains, Alaska, *Tectonophysics*, **367**, 1–11.
- Spada, G. (2003), *The Theory Behind TABOO*, Samizdat Press, Golden, Colo.
- Spada, G., et al. (2003), *TABOO, User Guide*, Samizdat Press, Golden, Colo.
- Spada, G., et al. (2004), Geodesy: Modeling Earth’s post-glacial rebound, *Eos Trans. AGU*, **85**(6), 62–64.
- Suito, H., and J. T. Freymueller (2009), A viscoelastic and afterslip post-seismic deformation model for the 1964 Alaska earthquake, *J. Geophys. Res.*, **114**, B11404, doi:10.1029/2008JB005954.
- Tarr, R. S., and L. Martin (1912), The earthquakes of Yakutat Bay, Alaska in September 1899, *U.S. Geol. Surv. Prof. Pap.*, **69**, 135 pp.
- Wessel, P., and W. H. F. Smith (1998), New, improved version of the Generic Mapping Tools Released, *Eos Trans. AGU*, **79**(47), 579, doi:10.1029/98EO00426.
- Wiles, G. C., D. J. Barclay, and P. E. Calkin (1999), Tree-ring-dated Little Ice Age histories of maritime glaciers from western Prince William Sound, Alaska, *Holocene*, **9**, 163–173, doi:10.1191/095968399671927145.
- Wolf, L. W., C. A. Rowe, and R. B. Horner (1997), Periodic seismicity near Mt. Ogden on the Alaska–British Columbia border: A case for hydrologically triggered earthquakes?, *Bull. Seismol. Soc. Am.*, **87**, 1473–1483.
- Zumberge, J. F., M. B. Heflin, D. J. Jefferson, M. M. Watkins, and F. H. Webb (1997), Precise point positioning for the efficient and robust analysis of GPS data from large networks, *J. Geophys. Res.*, **102**, 5005–5017, doi:10.1029/96JB03860.

J. L. Elliott, J. T. Freymueller, C. F. Larsen, and R. J. Motyka, Geophysical Institute, University of Alaska Fairbanks, 903 Koyukuk Dr., Fairbanks, AK 99775, USA. (julie@giseis.alaska.edu)